Modelling of Nuclear Fuel Behaviour

Paul Van Uffelen

Institute for Transuranium Elements

2006

The mission of the Transuranium Elements (ITU) is to protect the European citizen against risks associated with the handling and storage of highly radioactive elements. ITU's prime objectives are to serve as a reference centre for basic actinide research, to contribute to an effective safety and safeguards system for the nuclear fuel cycle, and to study technological and medical applications of transuranium elements, in support of EU policies.

A great deal of additional information on the European Union is available on the Internet.
It can be accessed through the Europa server
http://europa.eu

Printed in Germany

Abstract

The present document contains the lecture notes of P. Van Uffelen for his presentation in the session "Fuel Development needs" of the 2006 Frédéric Joliot & Otto Hahn Summer School on Nuclear Reactors - Physics, Fuels and Systems – organised from 23rd August until 1st September 2006 in Cadarache (France).

In order to ensure the safe and economic operation of fuel rods, it is necessary to be able to predict their behaviour and life-time. The accurate description of the fuel rod's behaviour, however, involves various disciplines such as nuclear and solid state physics, metallurgy, ceramics, applied mechanics and the thermal heat transfer. The strong interrelationship of these disciplines calls for the development of computer codes describing the general fuel behaviour. Fuel designers and safety authorities rely heavily on these types of codes since they require minimal costs in comparison with the costs of an experiment or an unexpected fuel rod failure.

The first part of the lecture dedicated to fuel behaviour modelling reviews the basic equations implemented in the fuel rod performance codes; namely, those for the heat generation and transfer from the center of the pellets to the coolant, the equations for the mechanical analysis of the fuel rod, and the equations for the behaviour of the gaseous fission products. In the second part of the lecture, advanced issues and future needs are discussed. Particular attention has been devoted to the probabilistic analysis in fuel performance calculations, to the role of the high burnup structure in UO_2 and MOX fuels, to the influence of the microstructure in mixed oxide fuels, and to the tendency to develop multi-time-scale approaches for both current and advanced nuclear fuels.

1. Introduction

1.1   Importance of fuel performance modelling

In order to ensure the safe and economic operation of fuel rods, it is necessary to be able to predict their behaviour and life-time. The accurate description of the fuel rod's behaviour, however, involves various disciplines ranging from the chemistry, nuclear and solid state physics, metallurgy, ceramics, and applied mechanics. The strong interrelationship between these disciplines, as well as the non-linearity of many processes involved calls for the development of computer codes describing the general fuel behaviour. Fuel designers and safety authorities rely heavily on these types of codes since they require minimal costs in comparison with the costs of an experiment or an unexpected fuel rod failure. The codes are being used for R&D purposes, for the design of fuel rods, new products or modified fuel cycles and to support loading of fuel into a power reactor, i.e. to verify compliance with safety criteria in safety case submissions.

In addition to steady-state irradiation, the fuel rod behaviour is also being simulated under transient and accident conditions, for example to assess the radiological source term. For the simulation of off-normal operating conditions, specific "accident" codes require an estimation of the fuel rod status prior to the accident, which is often pre-computed by means of a code for normal operating conditions (even though there is no fundamental difference). The present lecture will focus on the codes for normal operating conditions. The accident codes have been dealt with in the JFOH summer school of 2005.

1.2   Geometrical idealization and size of the problem

In principle, our spatial problem is three-dimensional (3D). However, the geometry of a cylindrical fuel rod (a very long, very thin rod) suggests that any section of a fuel rod may be considered as part of an infinite body, i.e. neglecting axial variations. By further assuming axial-symmetric conditions because of the cylindrical geometry, the original 3D problem is reduced to a one-dimensional one. Analysing the fuel rod at several axial sections with a (radially) one-dimensional description is sometimes referred to as quasi 2D or 1 1/2D. Most fuel rod performance codes fall into this category. Real 2D codes such as for instance the FALCON code [1] offer the possibility to analyse r-z problems (no azimuthal variation) and r-φ problems (no variation in axial direction). An example of a 3D code is TOUTATIS [2]. Generally, 2D or 3D codes are used for the analysis of local effects, whereas the other codes have the capability to analyse the whole fuel rod during a complicated, long power history.

In order to estimate the "size" of the problem at hand, the number of time steps must also be specified. For a normal irradiation under base load

4

operation, i.e. under no load follow operation, approximately 100-500 time steps are sufficient. However, for an irradiation in a research reactor like the OECD Heavy-water BWR in Halden many more variations of the linear rating with time are recorded. In such a situation, one must either simplify the complicated power history or increase the number of time steps to the order of several thousand. The simplest geometrical idealization needs approximately 20 radial and 20 axial nodes; a 2D representation of a single pellet would approximately need several hundred nodes. Therefore, local models, which are in almost all cases nonlinear, must be very carefully constructed, since even for the simplest geometrical idealization the number of calls may easily reach the order of millions:

15 radial x 15 axial nodes x 5000 time steps x 3 iterations = $3,4 \times 10^6$ calls

Even with the computer power of today, a full 3D analysis of, for instance, a real Halden history is practically impossible. In addition, such an analysis would also not be very meaningful, as the fuel fragments shape and position are determined by a stochastic process.

1.3 Uncertainties and limitations

In general, the uncertainties to be considered may be grouped into three categories. The first category deals with the prescribed quantities. The fuel rod performance code requires on input the fuel fabrication parameters (rod geometry, composition, etc.) and irradiation parameters (reactor type, coolant conditions, irradiation history, etc.). The second category of uncertainties is the material properties, such as the fuel thermal conductivity or the fission gas diffusion coefficients. The third and last category of uncertainties is the so-called model uncertainties. A good example of such an uncertainty is the plain strain assumption in the axial direction as illustrated in Figure 1, representing the interaction of the deformed and cracked fuel with the cladding. Intuitively, it is clear that for a detailed analysis of such problems 2D or even 3D models are indispensable.

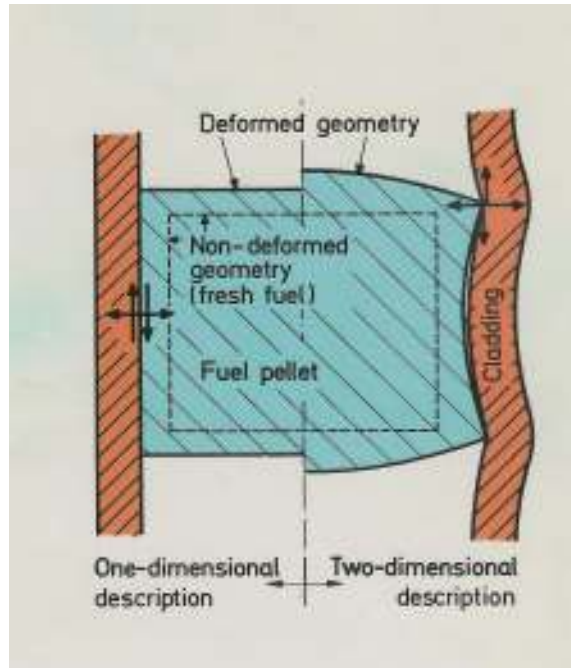**Figure 1: Schematic view of a deformed fuel pellet; comparison between a one-dimensional and a two-dimensional description.**

One of the most important consequences of all uncertainties is that one must implement models of "adequate" complexity.

2. Basic equations and state-of-the-art

2.1　　Heat transfer

The objective of this part is to describe how the temperature distribution in a nuclear fuel rod is calculated in a fuel rod performance code. The scope is limited to a description of the important physical phenomena, along with the basic equations and the main assumptions. Detailed numerical aspects as well as mathematical derivations are provided in some reference works [3-5].

The temperature distribution in a fuel rod is of primary importance for several reasons. First of all, the commercial oxide fuels have poor thermal conductivities, resulting in high temperatures even at modest power ratings. Secondly, the codes are used for safety cases where one has to show that no fuel melting will occur, or that the rod internal pressure will remain below a certain limit. Finally, many other properties and mechanisms are exponentially dependent on temperature.

The most important quantity is of course the local power density q''', i.e. the produced energy per unit volume and time. It is usually assumed that q''' depends only on the radius and the time. The linear rating is then simply given by

$$q' = \int_{r_{f,i}}^{r_{cl,o}} q'''(r)\, 2\pi r\, dr = \int_{r_{f,i}}^{r_{f,o}} \overline{q}_f''' \, f(r)\, 2\pi r\, dr + \int_{r_{cl,i}}^{r_{cl,o}} \overline{q}_{cl}''' \, 2\pi r\, dr \qquad (1)$$

where $r_{f,i}/r_{cl,i}$ is the inner fuel/cladding radius, $r_{f,o}/r_{cl,o}$ is the outer fuel/cladding radius, $\overline{q}_f'''$ and $\overline{q}_{cl}'''$ are the average power density in the fuel and cladding, respectively, and $f(r)$ is a radial distribution (form) function (cf. below). Generally, the linear rating is a prescribed quantity and is a function of the axial coordinate z and the time t. For some phenomena (e.g. cladding creep), the neutron flux is also needed. It can be prescribed as well but may also be calculated from the local power density q'''.

2.1.1　　Axial heat transfer in the coolant

In general three regimes must be covered in a LWR:
1. The sub-cooled regime, where only surface boiling occurs. This regime is typical for PWR's under normal operating conditions.
2. The saturated, two phase regime. This regime is typical for BWR's under normal operating conditions.
3. The saturated or overheated regime. This regime may be reached in all off-normal situations. A typical example is a LOCA.

The fuel rod performance codes use one-dimensional (axial) fluid dynamic equations that can only cope with the first two regimes. For simulating the

third type of regime, the whole reactor coolant system needs to be analysed by means of thermo-hydraulic system codes like RELAP or ATHLET.

The temperature calculation in the coolant serves two purposes. First of all, the axial coolant temperature in the basic (fictional) channel provides the (Dirichlet) boundary condition for the radial temperature distribution in the fuel rod. It results from the combined solution of the mass, momentum and energy balance equations. The simplified equation used in fuel performance codes reads

$$c\rho \frac{\partial T}{\partial t} + c\rho w \frac{\partial T}{\partial z} = q''_{cl,c} \frac{2\pi r_{cl,o}}{A} + q'''_{c} \tag{2}$$

where c represents the heat capacity, ρ the density, w the velocity , T the temperature, $q''_{cl,c}$ the heat flux from the cladding to the coolant, A the channel cross-sectional area, $r_{cl,o}$ the cladding outer radius and q'''_{c} the power density in the coolant. In general, the heat flux from cladding to coolant $q''_{cl,c}$ should be computed by means of a thermo-hydraulic code. Mathematically, the boundary condition is of the convective type:

$$q''_{cl,c} = -\lambda \frac{\partial T(r,t)}{\partial r}\bigg|_{r_{cl,o}} = \alpha \left\{ T(r = r_{cl,o}) - T_c \right\}$$

where α is the heat transfer coefficient between cladding and coolant and $T_c = T_c(z,t)$ is the (bulk) coolant temperature. Only for a steady-state condition

$$c\rho w \frac{dT}{dz} = \frac{q'}{A} + q'''_{c} \tag{3}$$

the heat flux from the cladding to the coolant is known and is given by

$$q''_{cl,c} = \frac{q'}{2\pi r_{cl,o}}$$

Under normal operational conditions, the mass flow rate $\dot{m} = A\rho w$, the coolant inlet temperature and pressure are prescribed. In an off-normal or accidental situation the normal operational condition is the initial condition, but the boundary conditions must be provided by the thermo-hydraulic system codes.

The second objective of the heat flow calculation in the coolant is the derivation of the radial temperature drop between the coolant and the cladding T_{cl}-T_c, resulting from convection:

$$q" = \alpha_{film}\left(T_{cl} - T_c\right) = \frac{q_c^{'''}}{2\pi r_{cl,o}}$$

The heat transfer coefficient in the film depends on the type of convection (forced or natural) and the type of coolant (gas, liquid, liquid metal). In the sub-cooled regime of a PWR, the Dittus-Boelter correlation is largely applied, whereas in the saturated regime of a BWR the Jens-Lottes correlation is applied (cf. separate lecture on thermohydraulics).

2.1.2   Heat transport through the cladding

The heat transport through the cladding occurs through conduction:

$$\frac{1}{r}\frac{\partial}{\partial r}\left(r\lambda_c\frac{\partial T}{\partial r}\right) + q_{cl}^{'''} = 0$$

where λ_c is the cladding conductivity (~ 20W/mK for Zircaloy), and the heat generation in the cladding is generally neglected (the gamma-heating, and well as the exothermic clad oxidation process are generally disregarded). In order to account for the presence of an outside oxide layer with a thermal conductivity on the order of 2 W/mK for ZrO_2 (thickness< 100μm), the total equivalent cladding conductivity can be obtained by applying the formula for serial thermal resistances. In a similar manner, the appearance of crud on the outer cladding surface is sometimes accounted for through an additional heat transfer coefficient.

2.1.3   Heat transport from cladding to the fuel pellet

The temperature difference in the pellet-cladding gap, ΔT_{gap}, is calculated as follows [6,7]:

$$\Delta T_{gap} = \frac{q''}{h_{gap}}$$

where q'' is the heat flux in W per unit area, h_{gap} is the heat transfer coefficient between fuel and cladding (gap conductance). Heat transfer by convection can be neglected. In general, the heat transfer coefficient h_{gap} depends on
1. gap width or contact pressure between fuel and cladding;
2. gas pressure and composition;
3. surface characteristics of cladding and fuel.

In fact, there are three parallel conduction routes:

$$h_{gap} = h_{rad} + h_{con} + h_{gas}$$

The contribution of the radiative component is given by

$$h_{rad} = \left(\frac{C_s}{\frac{1}{\varepsilon_f} + \frac{1}{\varepsilon_{cl}} - 1} \right) \frac{T_f^4 - T_{cl}^4}{T_f - T_{cl}}$$

where C_s is the Stefan-Boltzmann constant, ε the emissivity and T the temperature. The radiative component is less than 1% during normal operating conditions, because of the limited surface temperatures.

The component h_{con} reproduces the improvement in heat transfer due to contact pressure:

$$h_{con} = \alpha \bar{\lambda} \delta \left(\frac{P}{\delta^2 H} \right)^{\beta}$$

where $\bar{\lambda}$ and δ are the mean values of the thermal conductivity and the arithmetic mean roughness, respectively, P is the contact pressure, H is the Meyer hardness of the softer material, α and β are model parameters.

The heat transfer through conduction in the gas is often based on the model of Ross and Stoute:

$$h_{gas} = \frac{\lambda_{gas}}{\delta + s + g_f + g_{cl}}$$

where the thermal conductivity of a multi-component gas is only composition dependent and calculated by means of:

$$\lambda_{gas} = \sum_{j=1}^{n} \left[\frac{\lambda_j}{\left(1 + \sum_{\substack{k=1 \\ j \neq k}}^{n} w_{jk} \frac{c_k}{c_j} \right)} \right]$$

with c and w being molar concentrations and weighting factors respectively. The gas extrapolation lengths g_f and g_{cl} (or temperature jump distance) account for the imperfect heat transport across the solid-gas interface, which is material and gas-pressure dependent. Detailed formulations are discussed in [6,7].

It is important to note that, despite very detailed formulations for the gap conductance, there is an unavoidable uncertainty in the gap size s due to input uncertainties, but also because of uncertainties in the mechanical computation (e.g. cracking and fuel swelling, see below).

2.1.4 Heat transport in the fuel pellets

The heat produced by the slowing down of the fission fragments in the fuel pellets is removed through conduction in the pellets:

$$\rho c \frac{\partial T}{\partial t} = \frac{1}{r} \frac{\partial}{\partial r}\left(\lambda r \frac{\partial T}{\partial r}\right) + q''' \tag{4}$$

where c is the specific heat at constant pressure for fuel. The boundary conditions are

Inner boundary: $\quad \dfrac{\partial T(r = r_i, t)}{\partial r} = 0 \quad$ (radial symmetry)

Outer boundary: $\quad \Delta T_{gap} = \dfrac{q''}{h_{gap}}$ (pellet surface temperature is known)

The temperature distribution in the pellets is therefore affected by two terms: the heat source and the fuel thermal conductivity. At beginning of life (BOL), the heat production in LWRs is subject to a slight (typically in the range of 10%) depression, i.e. $q'''_{BOL} \square I_0(r)$, where $I_0(r)$ is the modified Bessel function. During the irradiation of the fuel, epithermal neutrons are captured preferentially near to the surface of the fuel by U^{238}. This leads to an enrichment of Pu^{239} at the outer periphery of the fuel. At end of life (EOL), $q'''_{f,o} \approx (2-3)\, q'''_{f,i}$, i.e. the power density distribution is a steep function of the radius (see Figure 2). This effect needs therefore to be considered and a specific model for the radial power density like TUBRNP is a prerequisite for any temperature analysis at high burn-up.
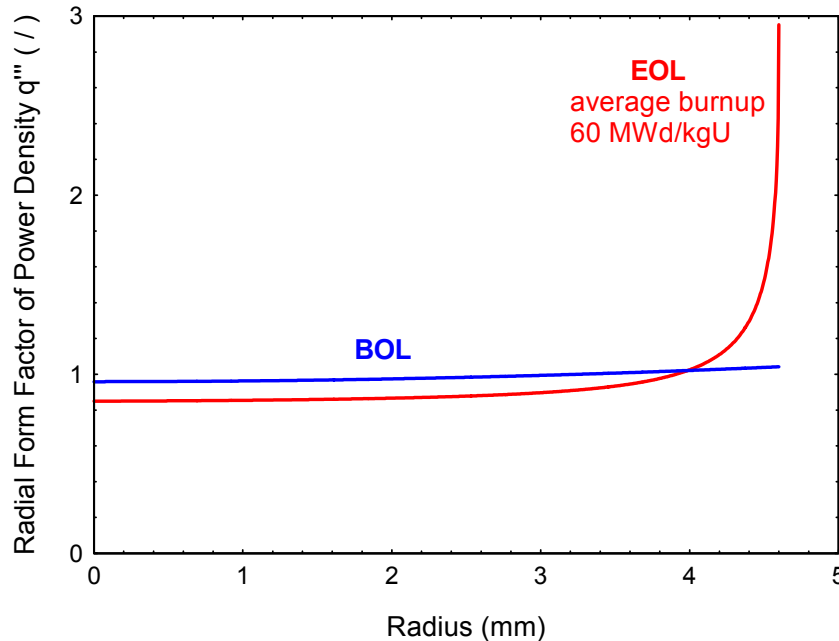

Figure 2: Radial form factor of the power density q''' at beginning and end of life for "typical" LWR conditions according to the TUBRNP model [8]. The radial distribution of the power density depends on enrichment, rod diameter, neutron spectrum and other parameters.

Conduction of heat in the pellets occurs by phonons or by the kinetic energy of electrons: $\lambda = \lambda_{ph} + \lambda_{el}$. At temperatures below 1500K the phonon contribution predominates. Above this temperature the electronic contribution becomes important. When applying the kinetic gas theory to the propagation of atomic vibrations (phonons) or quasi-particles, it appears that the phonon conductivity in the temperature range of interest can be expressed as

$$\lambda_{ph} = \frac{1}{A + B \cdot T}$$

where A corresponds to the scattering of phonons by imperfections such as point defects, line and planar defects, fission gas bubbles, etc. The parameter B corresponds to the scattering by phonon-phonon (Umklapp) interactions. When the burnup in the pellets increases, the accumulation of point defects and fission products will increase the phonon scattering (A-term). The same happens if the fuel (e.g. UO_2) is doped with a neutron absorber like Gd_2O_3, or if a deviation from stoichiometry occurs ($x \neq 0$, where x = $|$2-O/M$|$ and O/M is the oxygen-to-metal ratio in UO_2), i.e. in general A = A(bu, Gd, Pu, x).
The temperature dependent creation of electronic carriers leading to λ_{el} is typically expressed as:

$$\lambda_{el} = \frac{C}{T^2} \exp\left(-\frac{W}{kT}\right)$$

Besides the temperature and composition, the phonon contribution is also strongly dependent on the density. Several different formulations exist to account for the reduction of the thermal conductivity of theoretically dense fuel (λ_{TD}) with the porosity level (P) in the pellets:

Maxwell-Eucken: $\lambda = \lambda_{TD} \dfrac{1-P}{1+\alpha P}$ where α is a function of pore shape

Loeb: $\lambda = \lambda_{TD}(1 - \alpha P)$ where $\alpha = 1.7 - 3$

2.1.5   The structure of the thermal analysis

The structure of the thermal analysis in a fuel performance code can best be summarised as follows: The material properties λ, ρ and c are organised in an independent database whereas the power density q''', the gap conductance h_{gap} and the heat transfer coefficient between cladding and coolant α are formulated in a model. The "rest" is in a numerical algorithm, solving the heat conduction equation in the pellets and the convection problem in the coolant. A typical resulting temperature distribution calculated by means of the TRANSURANUS code is shown in Figure 3.
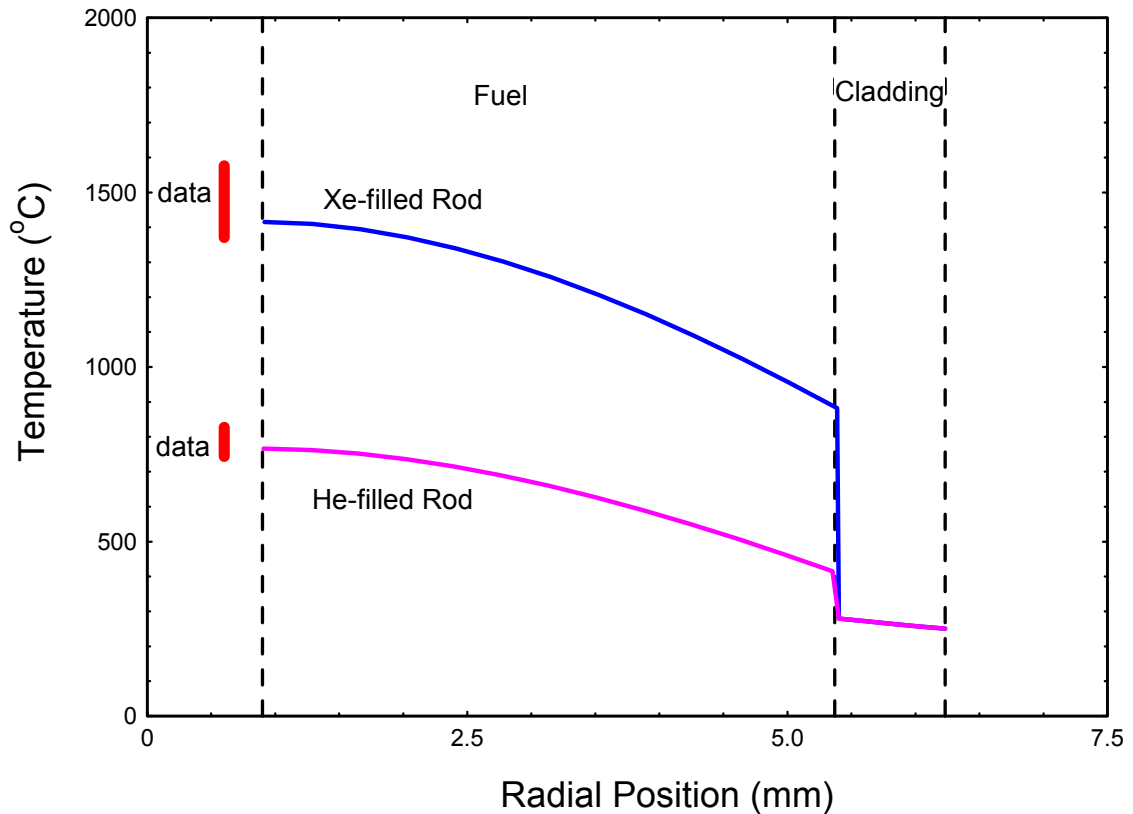
IFA-504; Linear Rating q' = 20 kW/m

Figure 3: Radial temperature distribution in a BWR-rod at begin of life. Comparison between the range of experimental results and predictions of the TRANSURANUS code for two different fill gases (He, Xe). The data refer to a thermocouple measurement in the central hole of the fuel pellet, indicated by the dashed line.

2.2   Mechanical analysis

The first barrier against release of radioactive fission products to the environment is the cladding of the nuclear fuel rod. The stress and associated deformation assessment of the cladding are therefore essential in fuel performance calculations. Furthermore, the deformation of both the pellets and the cladding affect the gap width, which in turn affects the conductance of the gap, hence the temperature distribution in the pellets. The thermal and mechanical analyses are therefore equally important and closely coupled. In principle, both problems should therefore be solved simultaneously. In practice, however, all fuel performance codes solve them separately but provide coupling through an iterative scheme. This important numerical aspect will not be dealt with in this lecture. The interested reader is referred to a general discussion on this issue in references [9-11].

The next sections summarise how stress and strains are calculated in both the ceramic pellets and the metallic cladding, while underlining the main assumptions and limitations.

2.2.1　Main assumptions and equations

The main assumptions generally made in fuel performance codes are
1. The system is axisymmetric, i.e. variables don't vary tangentially.
2. Although the fuel and cladding move axially (not necessarily at the same rate), planes perpendicular to the z-axis remain plane during deformation (plain strain condition), i.e. the rod remains cylindrical.
3. Dynamic forces are in general not treated, and the time dependence inherent in the analysis (creep) is handled incrementally.
4. Elastic constants are isotropic and constant within a cylindrical ring.
5. The total strain can be written as the sum of elastic and non-elastic components.

The first two assumptions reduce the problem to one dimension. The third assumption indicates that the stresses are related through a local equilibrium condition for the radial force in the following form:

$$\frac{d\sigma_r}{dR} = \frac{\sigma_t - \sigma_r}{R}$$

where σ_r and σ_t represent the normal radial and tangential stress, respectively, and R corresponds to the radius of the deformed geometry.

Since the fuel stack and cladding are treated as a continuous, uncracked medium, no discontinuities are allowed in their displacements. This is translated by the compatibility relations for the strains:

$$\begin{aligned}
\varepsilon_r &= \frac{du}{dR} \\
\varepsilon_t &= \frac{u}{R} \\
\varepsilon_a &= \text{constant} = C_3
\end{aligned} \qquad , \qquad (5)$$

where u represents the radial deformation and ε_i are the normal strains.

Finally, the last equation relates the stresses to the strains. Based on the fifth assumption, the constitutive relations read:

$$\underline{\varepsilon}^{\text{total}} = \underline{\varepsilon}^{\text{elastic}} + \sum \underline{\varepsilon}^{\text{non-elastic}} \qquad (6)$$

where

$$\underline{\varepsilon} = \begin{Bmatrix} \varepsilon_r \\ \varepsilon_t \\ \varepsilon_a \end{Bmatrix} \qquad (7)$$

2.2.2 Calculation of strains

Elastic strain

The elastic strains for an isotropic material are reversible and given by

$$\varepsilon_r^{elastic} = \frac{1}{E}\left[\sigma_r - \nu\left(\sigma_t + \sigma_a\right)\right]$$

$$\varepsilon_t^{elastic} = \frac{1}{E}\left[\sigma_t - \nu\left(\sigma_r + \sigma_a\right)\right].$$

$$\varepsilon_a^{elastic} = \frac{1}{E}\left[\sigma_a - \nu\left(\sigma_r + \sigma_t\right)\right]$$

Non-elastic strain

Thermal strain
The non-elastic strains consist of various contributions. First of all, there is the thermal strain resulting from temperature differences, which is assumed to be isotropic and reversible:

$$\varepsilon_i^t = \alpha \cdot \left(T - T_0\right) \quad i \in \{r, t, a\}$$

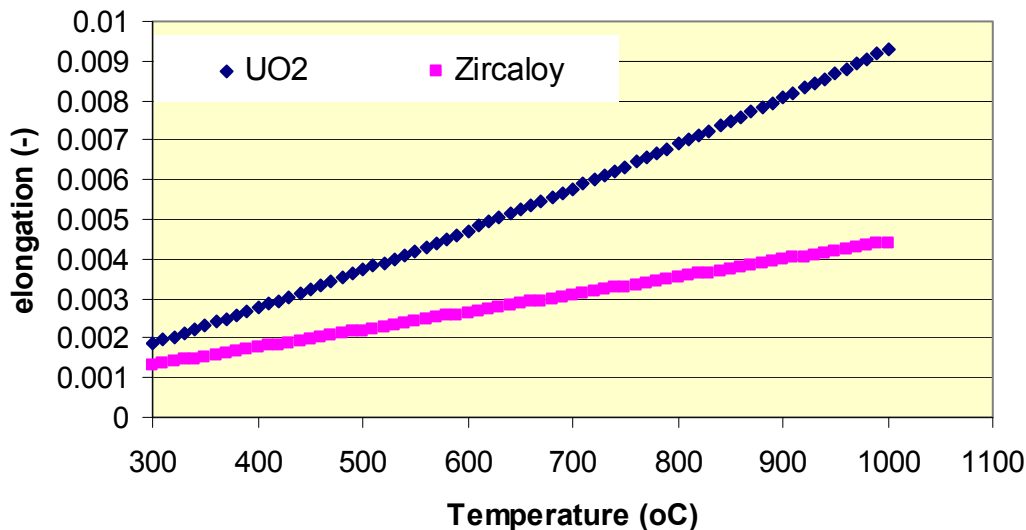The thermal expansion coefficients depend on the material and the temperature itself, as shown in the following figure

Figure 4: Elongation of UO$_2$ fuel and Zircaloy cladding due to thermal expansion (-), as a function of the temperature (^{o}C).

The larger thermal expansion of UO$_2$ with respect to that of zircaloy explains why thermal expansion is one of the largest contributions to the gap closure in a nuclear fuel rod at beginning-of-life.

Swelling

The second contribution to the non-elastic strain in the fuel pellets comes from swelling, and is also assumed to be isotropic. The fuel swelling in turn has four contributions:

$$\varepsilon^s_{fuel} = \frac{1}{3}\left[\left(\frac{\Delta V}{V}\right)_{solid\ FP} + \left(\frac{\Delta V}{V}\right)_{gaseous\ FP} - \left(\frac{\Delta V}{V}\right)_{densification} - \left(\frac{\Delta V}{V}\right)_{hot\ pressing}\right]$$

where the first term is attributed to the inexorable swelling of solid fission products:

$$\left(\frac{\Delta V}{V}\right)_{solid\ FP} = bu \cdot \left(\sum_{solid\ FP} Y_i \frac{v_i}{v_U} - 1\right)$$

which is linearly dependent on burnup, the fission product yield (Y_i) and on the partial volume of the species (v_i). In general the solid fission product swelling is on the order of 1% per 10 GWd/t. The second term comes from gaseous fission product swelling:

$$\left(\frac{\Delta V}{V}\right)_{gaseous\ FP} = \frac{4\pi}{3}\int_0^{R_{max}} R^3 N(R)\, dR$$

and requires a model to predict the gaseous fission product behaviour, more precisely the gas bubble formation due to the low solubility of rare gases in UO_2 (cf. below). During the initial stages of the irradiation (bu<10MWd/kgHM), the density increases as some fabrication porosity disappears as a result of the impact of fission fragments on the (small) pores. In general, the shrinkage process depends on the temperature, burnup, fission rate as well as combination of the initial density, the pore size-distribution and the grain size. The ideal situation is thus to have a fundamental model for densification, like those proposed by Assmann et al. [12] and Suk et al.[13]. However, values for the parameters involved are not always well known. Therefore many code developers have implemented empirical correlations for the fraction of the original porosity which has annealed out as a function of the local burnup, the temperature and the grain size, for example [14]:

$$\frac{\Delta P}{P_0} = \alpha\left[1 - \beta\exp(-a_1 \cdot bu) - (1-\beta)\exp(-a_2 \cdot bu)\right]$$

where α = (T^{o}C-83)/(288D$_{gr}$), $\alpha\beta$ = 5.12 exp(-5100/T^{o}K), a_2 = 0.0016 t_{UO2}/MWd, a_1 = 100 a_2. The densification, together with the solid fission product swelling is illustrated in Figure 5.
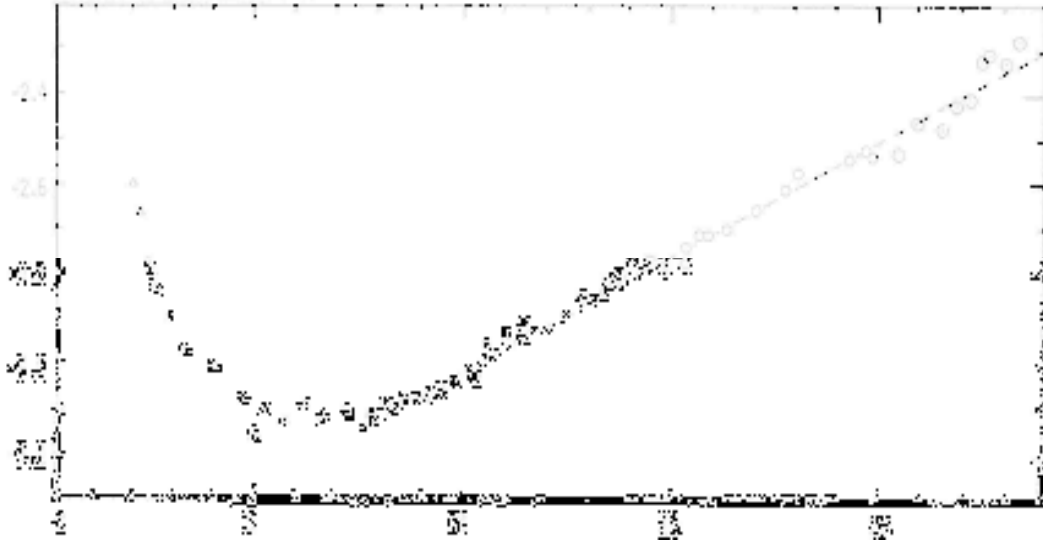
Figure 5: Change of the fuel pellet stack length (mm) at beginning-of-life as a function of the burnup (MWd/kgUO2), showing the combined effect of densification and solid fission product swelling.

Under the influence of large temperatures, stress levels and defect production rates during irradiation, a fraction of the fabrication porosity will disappear. This fourth contribution to fuel swelling is referred to as hot pressing and is similar to creep (see below). Therefore, either vacancy diffusion

$$\frac{dP}{dt} = -K \left(\frac{\Omega D_{vol}}{kT} \right) \frac{P}{R_{gr}^2} \sigma$$

or plastic flow (i.e. dislocation climb or other model of creep)

$$\frac{dP}{dt} = -\frac{9}{4} \alpha \sigma P$$

are considered.

The isotropic swelling strain in the cladding is due solely to void formation, hence it requires a model for the evolution of voids in the metal.
Plasticity and creep
The third contribution to the non-elastic strain in the fuel is visco-plastic in nature. It consists of instantaneous plastic deformation when the yield stress is exceeded and of time-dependent creep. For the fuel and cladding a simple isotropic plastic flow model can be applied. Nevertheless, as creep is the main contributor to stress relaxation after cracking (see below) in the oxide pellets, it is often only considered in the cladding.
In a multiaxial state of stress a method of relating the onset of plastic deformation to the results of a uniaxial test is required. Furthermore, when plastic deformation takes place one needs to determine (1) how much plastic deformation has occurred and (2) how that deformation is distributed among the individual components of strain. For the first requirement a so-called yield-

function is needed. This may be one-dimensional like the Mises criterion [15,16]:

$$\sigma_{eff} = \frac{1}{\sqrt{2}} \left[\left(\sigma_r - \sigma_t \right)^2 + \left(\sigma_r - \sigma_a \right)^2 + \left(\sigma_t - \sigma_a \right)^2 \right]^{\frac{1}{2}}$$

so that yielding only occurs when the effective or equivalent stress (σ_{eff}) exceeds the yield stress determined from a uniaxial tensile test. Others have introduced the anisotropic factors according to Hill's methodology [5]. Finally, a multidimensional yield surface [17,18] has also been proposed. In order to account for work hardening, one generally assumes that the yield stress changes with the total permanent deformation. The plastic strain is therefore computed incrementally.

In order to answer the second question, each increment of effective plastic strain is related to the individual plastic strain components by a flow rule:

$$\Delta \varepsilon_i = \Delta \varepsilon_{eff} \frac{\partial \sigma_{eff}}{\partial \sigma_i} \qquad i \in \{r,t,a\}$$

When using the above mentioned definition of the equivalent stress, one obtains the Prandtl-Reuss flow rule:

$$\Delta \varepsilon_i^p = \frac{3 \Delta \varepsilon_{eff}^p}{2 \sigma_{eff}} S_i \qquad i \in \{r,t,a\}$$

indicating that the plastic strain increment is proportional to the deviatoric stress $S_i = \sigma_i - \sigma_h$ where $\sigma_h = (\sigma_r + \sigma_t + \sigma_a)/3$.

For the time-dependent creep one needs strain rate equations, although the total creep strain is also computed incrementally by multiplying the strain rate with the time step length. For primary creep, typically an empirical expression is applied:

$$\dot{\varepsilon}_{eff} = K \sigma_{eff}^n t^m$$

where K, n, m are constants.

For the secondary or steady-state creep, there are three parallel processes. The vacancy diffusion or Nabarro-Herring creep and the dislocation climb are dominating at high temperature and high stresses, respectively:

$$\left(\dot{\varepsilon}_{eff}^c \right) = \frac{B q'' \sigma_{eff}}{R_{gr}^2} \exp\left(-\frac{E_d}{kT} \right) \qquad \text{vacancy diffusion}$$

$$\left(\dot{\varepsilon}_{eff}^c \right) = B' q'' \sigma_{eff}^{4.5} \exp\left(-\frac{E'_d}{kT} \right) \qquad \text{dislocation climb}$$

The third process is irradiation induced creep, dominating at low temperatures and assumed to be proportional to the effective stress and the local fission rate density or q'''.

18

Pellet cracking

The fourth and last non-elastic strain component stems from the pellet cracking. Pellet cracking already occurs at startup due to the differential thermal expansion since the hot pellet centre expands more than the cold periphery. In order to assess the linear heat generating rate at which cracking in cylindrical pellet occurs, the maximum thermal stress (= $\sigma_{t,max}$ = $\sigma_{a,max}$ at pellet periphery) in an uncracked pellet submitted to a parabolic temperature gradient

$$\sigma_{t,\max} = -\frac{\alpha E q'}{8\pi(1-\upsilon)\bar{\lambda}},$$

must be compared with the (uniaxial) fracture stress, which is approximately 130 MPa. When using E=200 GPa, υ=0.31, the thermal diffusivity α=10^{-5} K^{-1}, and an average thermal conductivity of λ=3 W/mK radial cracks are predicted to be initiated in the pellet periphery at a linear heat rate q' of the order of 5 kW/m. The number of cracks (N_{cr}) is dependent on the linear hear rate. Oguma [19] proposed a linear model for the number of radial cracks that is illustrated in Figure 6. In addition to radial, also axial and (especially under ramping conditions) circumferential cracks are formed.
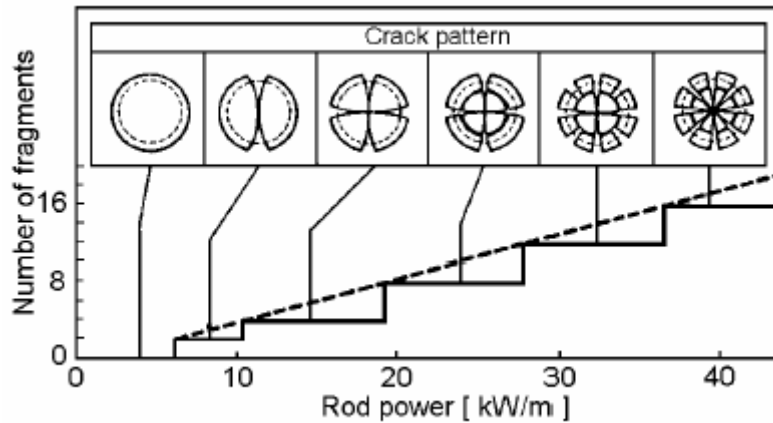

Figure 6: Calculated crack pattern from thermoelastic stress [19]

The consequences of cracking are very important in fuel performance modelling. Owing to the larger thermal expansion of the fuel fragments in comparison with that of a monolithic cylinder, and due to vibration induced motion they move outwards. This is called pellet "relocation" and has a strong impact on the thermal behaviour as shown in Figure 8. It reduces the pellet-cladding gap size, thereby reducing the temperature levels in the fuel at beginning-of-life. This constitutes the largest contribution to the gap closure (approximately 30-50%, depending on q') but is also the one which is subject to the largest uncertainty, because of the stochastic nature of the cracking process. This also raises questions about the usefulness of applying 3D stress calculations.

The contribution from relocation is generally accounted for in the tangential strain component as a (linear) function of the linear heat rate: ε_t = u/r, where u

= $s\delta_g$, s being the initial radial gap size and δ_g the fraction of the gap size closing as a result of relocation. An example based on the relocation model in the FRAPCON3 code [20] is illustrated in Figure 7 [21].
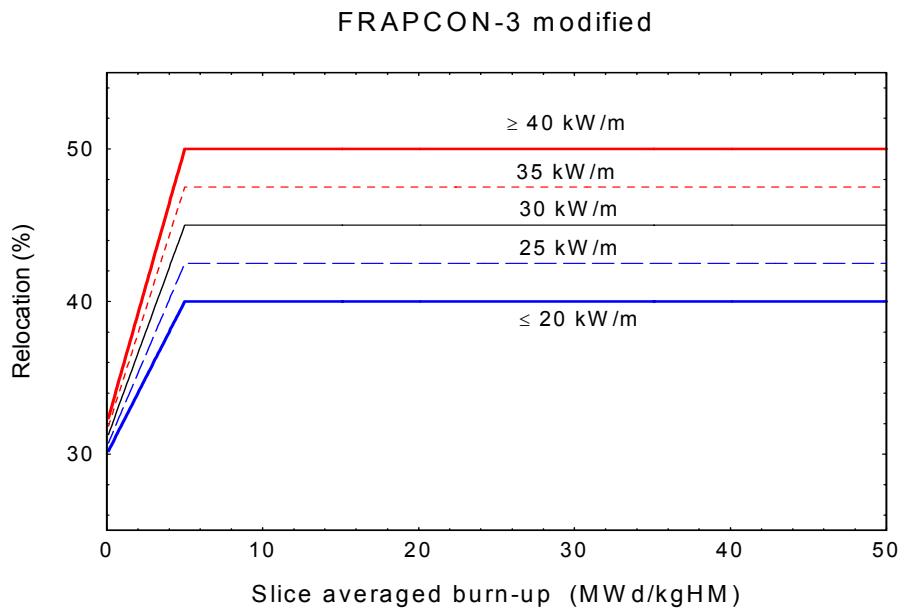
FRAPCON-3 modified

Figure 7: Fraction of gap closure due to pellet fragment relocation (δ_g), derived from the relocation model in the FRAPCON3 code.

When the pellets swell large enough so that they come into contact with the cladding, which creeps down under influence of the pressure difference between the coolant pressure and the fill gas pressure, then relocation may be (partly) reversed.

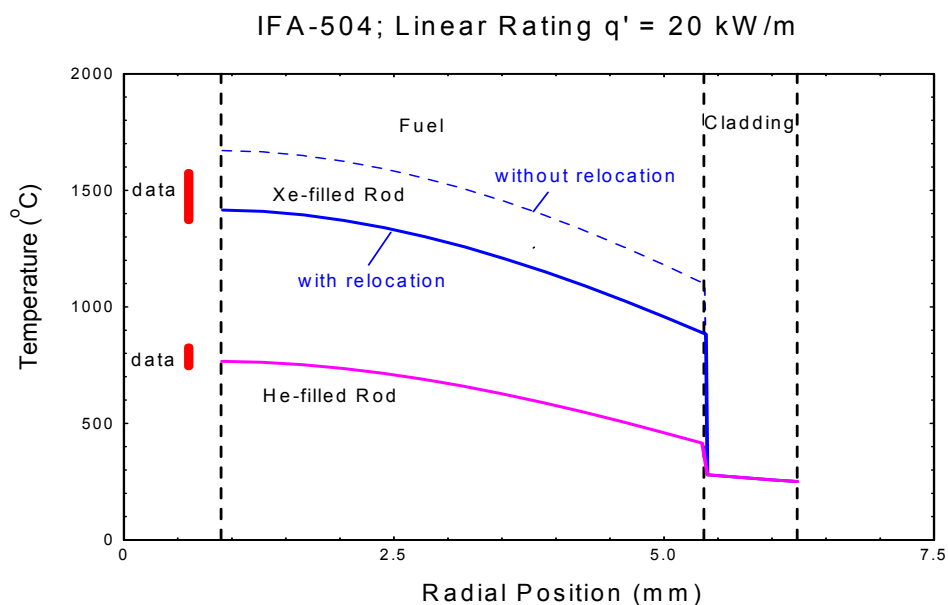**IFA-504; Linear Rating q' = 20 kW/m**

Figure 8: Radial temperature distribution in a BWR-rod (IFA-505) at beginning of life calculated by the TRANSURANUS code. Comparison between the analysis of a Xe-filled rod with (full line) and without (dashed line) taking relocation into account.

20

The effect of relocation on the mechanical behaviour is also of primary importance since it reduces the overall stress in the pellets and may even change the sign of the stress in pellet centres from compression (in a cylinder) to traction (in fragments)[22]. To account for the cracks exactly would require the exact location and size of every crack and to solve a 3D stress-strain problem in each block. Instead, one simply modifies either the material constants [16,21] or modifies the constitutive equations. An example of the former approach is that of Jankus and Weeks [23], where a reduction of the elastic constants is proposed:

$$E' = \left(\frac{2}{3}\right)^{N_{cr}} E$$

$$v' = \left(\frac{1}{2}\right)^{N_{cr}} v$$

which means that an equivalent continuous and homogeneous solid body with directionally dependent (anisotropic) properties is considered. As the pellet-clad gap closes during irradiation the contact pressure can press the fragments inward, thereby reducing the relocated radius to a minimum value. Some codes also account for the restoration of the elastic constants as the relocation is reversed (partially) [16].
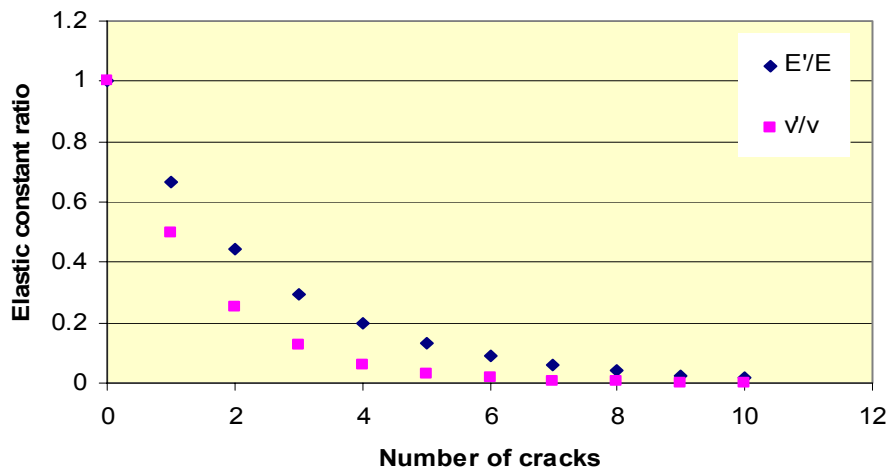

Figure 9: Effect of the number of cracks on the elastic modulus and the Poission's ratio according to Jankus et al.[23]

In order to modify the constitutive equations, a plane stress condition has been proposed [17], i.e. the tangential stress is set equal to the fill gas pressure once the radial crack appears. Both types of approaches, however, do not account for crack healing.

2.2.3 Boundary conditions

In order to solve the main equations summarized in section 2.2.1, boundary conditions are required.

Radial boundary conditions

In general, continuity of the radial stress and displacement at each radial zone is imposed and the radial stress at the outer cladding surface is determined by the coolant pressure: $\sigma_r(r_{cl,o}) = -p_{cool}$.

The boundary condition in the rod depends on the configuration. When pellet-cladding mechanical interaction is not established, the radial stress at the pellet periphery is determined by the fill gas pressure in the fuel rod (p_{gas}): $\sigma_r(r_{f,o}) = -p_{gas}$. For the boundary condition in the pellet centre, two possibilities exist. In hollow pellets, the radial stress at the pellet centre is equal to fill gas pressure as well: $\sigma_r(r_{f,i}) = -p_{gas}$, whereas in the event of full cylindrical pellets the radial and tangential stresses are equal in the pellet centre.

When the fuel and cladding are in contact, a fuel pellet interfacial pressure exists (p_{fc}) and determines the boundary condition at the pellet surface: $\sigma_r(r_{f,o}) = \sigma_r(r_{cl,i}) = -p_{fc}$. The other radial boundary conditions remain unchanged.

Axial boundary conditions

The plane strain assumption entails that the axial strain is constant in the plane perpendicular to the axial axis. The axial strain is therefore determined by an axial force balance equation including the fill gas pressure, the plenum spring pressure, the fuel column weight and the friction forces. The latter depend on the fuel-cladding interaction and can only be taken into account iteratively. Indeed, when a section i is analysed it is not known whether friction forces between fuel and cladding originating from a section above/below i need to be considered in the axial balance of forces. This is schematically shown in Figure 10. In the case of a radial contact between fuel and cladding both bodies may stick to each other, but some sliding may be possible in specific conditions (sticking or static vs. sliding friction). Part of the fuel rod may be "trapped", which means that rather high axial forces may act on cladding and fuel.

One advantage of 2D and 3D finite element models is that such effects are automatically included in the analysis through the use of specific gap elements.
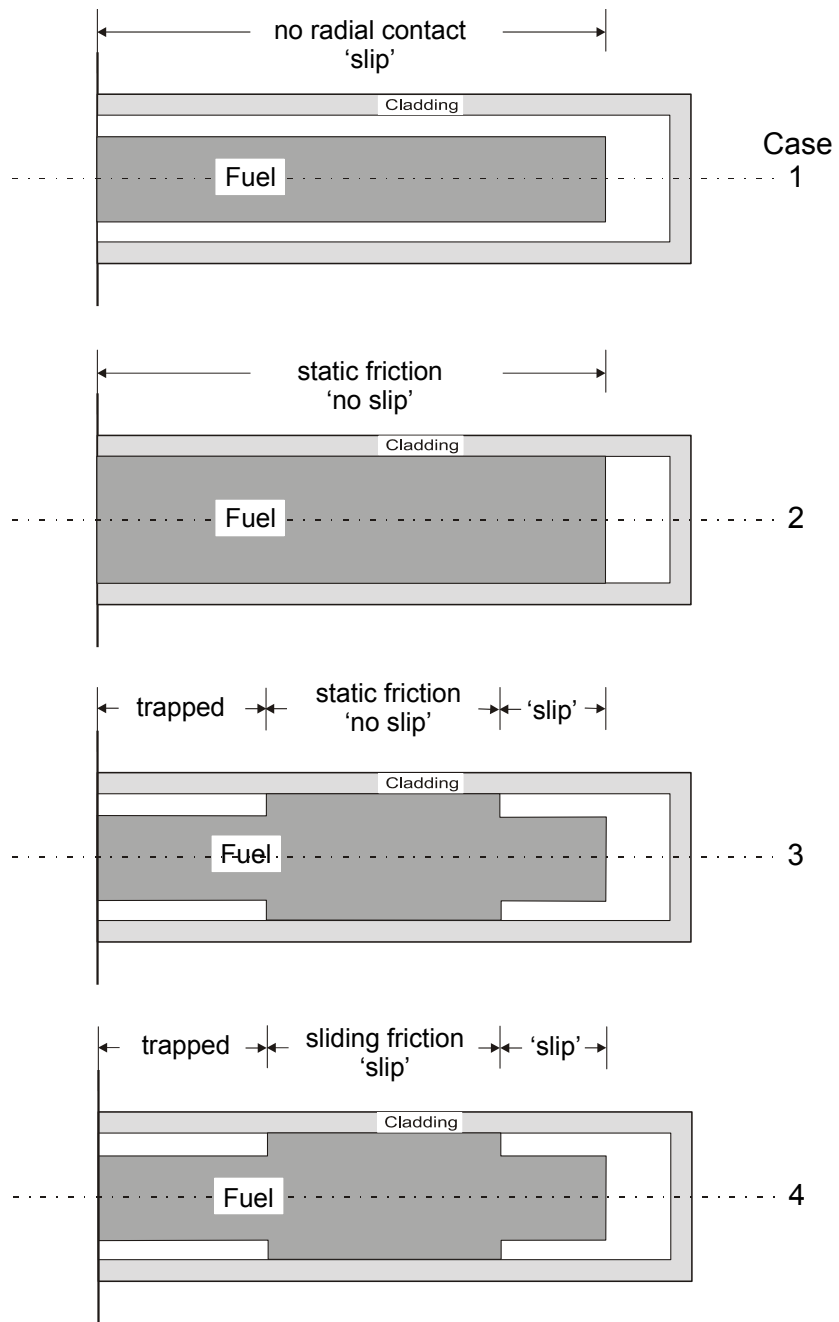
Figure 10: Four possible modes of an interaction between fuel and cladding.

2.3 Fission gas behaviour

On average each fission event produces 0.3 Xe and Kr atoms. These inert fission gas atoms have a very low solubility limit (~0.3 wt% for Xe) causing two important life-limiting phenomena in the fuel rod: either they remain in the pellets and contribute to the swelling, or they are released from the pellets and increase the rod internal gas pressure while reducing the thermal heat transfer in the gap. The fuel swelling may lead to pellet cladding mechanical interaction and even cladding failure under certain conditions. Likewise, the fission gas release may lead to higher fuel rod temperatures, which in turn could lead to higher fission gas release until the rod fails due to clad ballooning and clad burst.

Because of its implications for fuel performance, the basic mechanisms involved in the fission gas release and swelling in LWR fuel will be summarised first, before outlining how these phenomena are implemented in a code. The interested reader will find more details in [24].

2.3.1 Basic mechanisms

Recoil, knockout and sputtering
In general, a fission event entails – among others – two fission fragments that convey their kinetic energy to the fuel lattice. A fission fragment, close enough to a free surface (< 6-7 microns), can escape from the fuel due to its high kinetic energy (60-100 MeV). This is called recoil release. When fission fragments make elastic collisions with the nuclei of lattice atoms, a collision cascade appears. The interaction of a fission fragment, a collision cascade or a fission spike with a stationary gas atom near the surface can also cause the latter to be ejected if it happens within a distance close enough to the surface. This process is called release by knock-out. Finally, a fission fragment travelling through oxide looses energy, causing a high local heat pulse. When this happens close to the fuel surface, a heated zone will evaporate or sputter, thereby releasing any fission product contained in the evaporated zone.
Recoil, knockout and sputtering can only be observed at temperatures below 1000°C, when thermally activated processes (cf. below) do not dominate. They are almost temperature independent and therefore called athermal mechanisms. It is generally of little importance in reactor at intermediate burnup levels. The fraction of athermal release is roughly under 1% for rod burnups below 45 MWd/kgU, and accelerates to roughly 3% when the burnup reaches about 60 MWd/kgU.

Lattice diffusion of single gas atoms
The first and basic step in fission gas release is single gas atom diffusion in the lattice. Possible mechanisms by which the inert gas atoms migrate through the fuel have been studied by Grimes [25] by considering low energy migration pathways between solution sites as well as the stability of gas atoms at a variety of solution sites within a defective UO$_{2\pm x}$ lattice (x=| O/M-2|, the deviation of the stoichiometry). He postulates a cation vacancy controlled

migration pathway for Xe atoms. Indeed, according to his calculations, Xe is trapped at a uranium vacancy in UO_{2+x}, at a tri-vacancy cluster in UO_{2-x} and at a di -or tri-vacancy in UO_2. Since the local environment of the migrating Xe atoms is supposed to become the charged tetra-vacancy for all stoichiometries, the mechanism for diffusion only considers the association of a cation vacancy to the trap sites.(Uranium vacancies as the slower moving species are rate-controlling for most diffusion related processes in UO_2).
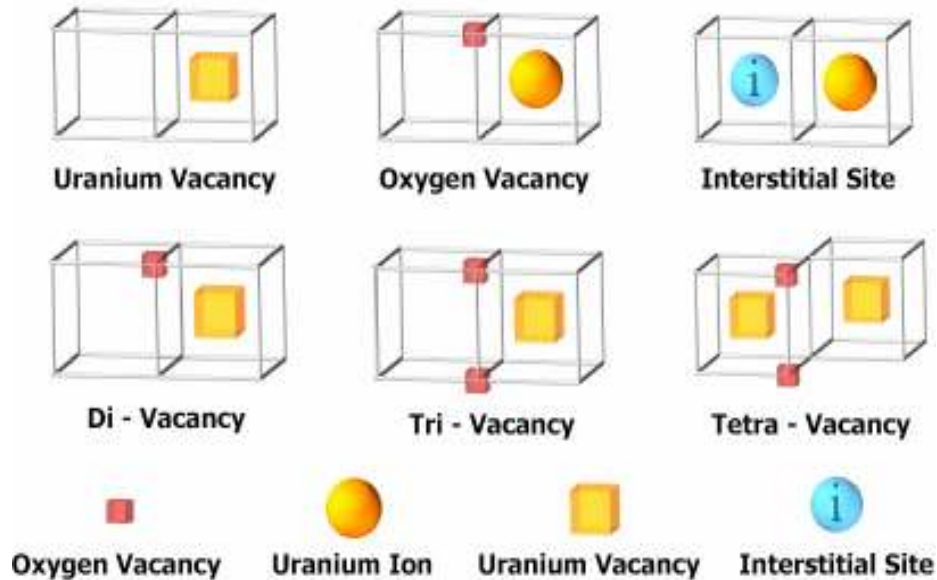

Figure 11: Possible solution sites for fission products in $UO_{2\pm x}$ according to Grimes [25]

The lattice diffusion coefficient is influenced by the temperature, deviations from stoichiometry and additives (e.g. Cr, Nb), phase changes and therefore also indirectly by the burnup. Also the fission fragments are assumed to contribute to the diffusion process, which is referred to as irradiation enhanced diffusion. This is due to the interaction of the fission fragments and the associated irradiation damage cascades with the fission gas atoms in the lattice, resulting in a displacement of the gas atoms. This effect dominates the diffusion process at temperatures below $1000^{\circ}C$ and is temperature independent. For temperatures between $1000^{\circ}C$ and $1400^{\circ}C$, vacancies necessary for the gas atom diffusion are assumed to be created both thermally and by the damage cascades related to fission fragments. Above $1400^{\circ}C$, a purely thermally activated diffusion coefficient is applied, i.e. thermally created vacancies for diffusion are predominant. These three temperature regimes are reflected in the three components of the single gas atom diffusion coefficient (m^2/s) often applied in the fuel performance codes [26]

$$D = D_1 + D_2 + D_3$$

where

$$D_1 = 7.6 \cdot 10^{-6} \exp\left(-\frac{35000}{T}\right)$$

$$D_2 = 5.6 \cdot 10^{-25} \cdot \sqrt{\dot{F}} \exp\left(-\frac{13800}{T}\right)$$

$$D_3 = 8 \cdot 10^{-40} \cdot \dot{F}$$

where $\dot{F}$ is the fission rate density and T is the absolute temperature.

Unperturbed (intrinsic) diffusion of single inert gas atoms (Xe, Kr) can be observed at low damage and gas concentration (10^{-5} at-%). At higher gas and damage concentrations other effects should be taken into account.

Trapping
In nuclear fuels, either natural (e.g. impurities, dislocation lines, closed pores, etc.) or radiation produced imperfections in the solid (e.g. vacancy clusters in fission tracks, fission gas bubbles, solid fission product precipitates, etc.) depress the amount of fission products available for diffusion by temporarily or permanently trapping the migrating atoms. The experiments show that for burnups characteristic of power reactors, gas atom trapping due to (intragranular) fission gas bubbles in the grains is predominant. The trapping rate depends on the size of the intragranular bubbles, hence on temperature, fission rate and burnup. A second important effect of trapping occurs at grain boundaries. It deals with the delay for the onset of thermal fission gas release, via the bubble interconnection mechanism (cf. below).

Irradiation induced resolution
A fraction of the gas atoms trapped in bubbles can be re-dissolved in the surrounding matrix through the interaction of a fission fragment with the bubble. Two different types of mechanisms are proposed to explain the experimental observations. On one hand, microscopic models consider the resolution of one gas atom at a time when interacting with a fission fragment or an energetic atom from the collision cascade. Macroscopic models on the other hand consider the complete bubble destruction, but there is still discussion about the detailed mechanisms. For (larger) grain boundary bubbles resolution is supposed to be less effective.

Grain boundary diffusion
Grain boundary diffusion is the most commonly observed route for solute migration in polycrystalline materials. It is generally accepted that diffusion in crystalline solids proceeds more rapidly along grain boundaries than through the lattice. This is due to the atomic jump frequency in these planar defects which is about a million times greater than the jump frequency of regular lattice atoms in stoichiometric materials at 0.6 times the absolute melting temperature. Nevertheless, there is a switch from release assisted by grain boundary diffusion in trace-irradiated UO_2 to trapping and eventual interlinkage of the intergranular bubbles (cf. below). This switch occurs early in life, so that grain boundary diffusion is only considered to contribute to the precipitation of fission gas atoms in grain boundary bubbles, rather than to the

long range transport along grain boundaries to the free surface of the pellets [27].

Grain boundary sweeping or grain growth
In LWR fuel under normal operating conditions, only normal grain growth is observed, i.e. large grains grow at the expense of smaller ones. It affects fission gas release in two ways. First of all, grain boundary sweeping provides another mechanism for the collection of gas at these internal surfaces from which release can occur. The collection results from the low solubility of the fission gas, hence the sweeping grain boundary does not redeposit any gas in the newly formed crystal behind it. The moving grain boundary acts as a fission gas filter.
Secondly, the average diffusion distance for the fission products created in the grain increases. Unlike the first consequence this tends to reduce the release rate.
Grain boundary sweeping occurs at temperatures above roughly 1600°C.

Bubble migration
The migration of fission gas bubbles provides an alternative to the sequence "bubble formation-resolution-gas atom diffusion" in order to describe fission product release from nuclear fuels. Migration of bubbles in the oxide fuels has two other important consequences, namely the columnar grain growth with the concomitant central void formation (observed in fast breeder reactor fuel), and the coalescence of the bubbles which gives rise to fuel swelling.
Under normal operating conditions, however, fission gas bubbles remain small (typically below 20 nm) due to resolution, and show a small mobility at least up to 1800°C [28]. This is partly explained by the pinning by dislocations and other crystal defects.

Bubble interconnection
Fission gas bubbles appear along grain boundaries after a certain burnup, depending on the temperature history. When bubbles interconnect, they form a so-called tunnel network through which the gas can be released. The bubble interconnection is a reversible process, for the tunnel network can close again under the influence of the surface tension when the outgoing flux of gas atoms outweighs their supply.
The bubble interconnection has two important consequences. First of all, it determines the onset of release as the release remains small (due to athermal release) before grain boundary bubbles interconnect with open grain edge tunnels. This incubation period is reflected in the Vitanza threshold for fission gas release, which is shown in Figure 12. The ensuing release corresponds to a seepage process. Secondly, when grain face bubbles interconnect and form snake-like tunnels, there will be a sudden release of the gas accumulated in these bubbles, referred to as burst release. This can also be interpreted as a sudden interconnection or opening of grain face bubbles due to micro-cracking along grain boundaries during abrupt power variations. Cracking entails a sudden opening of a fraction of the grain boundaries with the instantaneous venting of the corresponding fraction of the accumulated gas atoms.

Interconnection of gas filled bubbles takes place in general where diffusion controlled precipitation occurs at the grain boundaries, i.e. when both T and the burnup are high enough. The conditions correspond roughly to the Vitanza threshold [29,30]:

$$T_c \left({}^o C \right) = \frac{9800}{\ln\left(\dfrac{bu}{0.005} \right)}$$

where T_c represents the central temperature in degrees Celcius, and bu the burnup in MWd/kgUO$_2$.
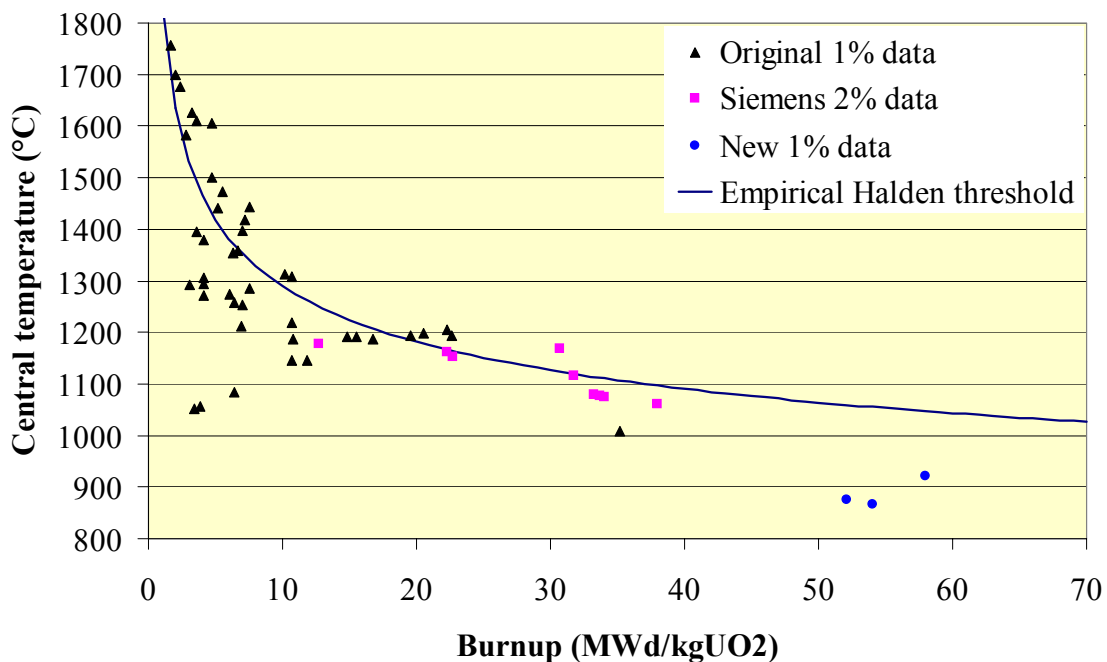

Figure 12: Original Vitanza criterion for the onset of fission gas release and supporting data [29,30].

2.3.2   *Modelling the fission gas behaviour*

There are various approaches in fission gas release and swelling modelling. They can be classified in two categories. On one hand there are purely empirical models, including those based on soft computing techniques such as neural networks. These models are inexpensive to use and provide an efficient tool for the design of fuel rods within a limited range of application. However, they are not suitable for gaining knowledge about the underlying mechanisms, nor do they enable us to extend their range of application to higher discharge burnup values as required by the industry. On the other hand, there are mechanistic models which aim at the physical description of the underlying phenomena. Despite their great data needs, such models provide an excellent basis, both for the analysis of the mechanisms, as well as for the extension of the models beyond their range of calibration.

Fuel performance codes nowadays tend to implement more and more mechanistic models, based on very detailed but stand-alone models. They all consider fission gas release to be a two-step process. The first step deals with the gas behaviour in the grains (intragranular part), whereas the second step deals with the gas behaviour along the grain boundaries (intergranular part).

Intragranular behaviour
For the behaviour in the fuel grains, the following scenario is generally adopted. The gas atoms are created by fission in the fuel matrix. They then diffuse in the grains towards grain boundaries by thermal and irradiation enhanced diffusion. Small intragranular bubbles with a diameter of 1 to 2 nm are observed in irradiated fuel. They are created in the wake of fission spikes and then grow by diffusion (trapping). They are continuously destroyed by fission spikes (resolution). There is no bubble migration except at temperatures above roughly 1800°C. The bubbles act as sinks for gas atoms, thereby reducing the amount of gas available for release.

This scenario leads to solving a diffusion equation in a sphere with a source term proportional to the local fission rate density ($S = Y_{fp}\dot{F}$), which is based on the pioneering model of Booth [31]. He proposed the equivalent sphere model. This theory considers a polycrystalline sinter as a collection of uniform spheres with an equivalent radius in order to simplify the mathematical problem. The hypothetical sphere radius (R_B) is defined so that the effective surface-to-volume ratio of the fuel (*S/V*) is preserved:

$$R_B = 3\left(\frac{V}{S}\right)_t$$

where *(S/V)$_t$* accounts for the sum of the geometric surface of the pellets as well as the surface due to open porosity. As irradiation proceeds, fission gases are generated within the Booth sphere and migrate to the surface, where the concentration is taken to be zero. He proposed that the fractions of stable gas release can be approximated by

$$f_{ann}(t) \simeq 6\sqrt{\frac{Dt}{\pi R_{gr}^2}} - 3\frac{Dt}{R_{gr}^2}$$

for so-called annealing conditions (i.e. without source term, but with an initial non-zero concentration), and

$$f_{irr}(t) \simeq 4\sqrt{\frac{Dt}{\pi R_{gr}^2}} - \frac{3}{2}\frac{Dt}{R_{gr}^2}$$

for irradiation conditions (non-zero source term, but no initial concentration). In a second model he proposed the approximation for the release-to-birth ratio for unstable gas release under steady-state conditions [32]:

$$\frac{R}{B} = \frac{3}{R_{grain}} \sqrt{\frac{D}{\lambda}} \left[\coth\left(R_{grain} \sqrt{\frac{\lambda}{D}} \right) - \frac{1}{R_{grain}} \sqrt{\frac{D}{\lambda}} \right]$$

where λ represents the decay constant of the species under consideration. It should be underlined that **the diffusion coefficient to be used is subject to an order of magnitude uncertainty**. The expression in section 2.3.1 is often being used, with a multiplication or reduction factor of about 5.

Regardless of the uncertainty on the diffusion coefficient, the Booth models themselves suffer several limitations:
1. they consider a constant temperature and fission rate density
2. they do not account for resolution and trapping at intragranular bubbles
3. they do not account for grain boundary sweeping
4. they cannot reproduce an incubation period (cf. Vitanza curve)
5. they do not account for resolution at grain boundary bubbles

All of these limitations have been alleviated over time. First, several numerical techniques have been proposed to cope with time-varying conditions, which have been compared in ref. [33]. In order to deal with trapping and resolution, Speight [34] found that instead of solving one diffusion equation coupled with an equation for the gas balance in the traps, one could solve a single diffusion equation for the sum of the concentration in the matrix and in the traps with an effective diffusion coefficient (D_{eff}):

$$D_{eff} = D \frac{b}{b+g}$$

where $g = 4\pi R_{bubble} D$ corresponds to the trapping rate coefficient and b corresponds to the resolution rate coefficient. Whatever model is being considered for resolution, fission gas behaviour models generally introduce a simple resolution rate coefficient that is proportional to the local fission rate density and depends on the bubble size:

$$b = 2\pi \left(R_{bl} + \delta \right)^2 \mu_{ff} \dot{F}$$

where it is assumed that a bubble can be destroyed if its centre lies within a distance δ from the fission fragment track of length μ_{ff} = 7-10 microns. The condition for applying $D_{eff,}$ is that the traps are saturated. Experiments show that small intragranular bubbles stabilize rapidly both in size and in diameter. Intragranular bubbles can therefore be considered saturated for irradiation times of practical interest (beyond 0.5 MWd/kgU). Nevertheless, the difference between D and D_{eff} is only important for temperatures above approximately 1100°C. It should be underlined, however, that during a power ramp the application of D_{eff} provides an overestimation of the trapping effect [35].

Over time, several models have been proposed wherein the Booth sphere radius was taken to be equal to the average grain radius of the fuel, in order to be able to account for grain growth. However, it must first be pointed out that

there is no consensus about which grain growth model should be applied, even though the Ainscough [36] model is often applied:

$$\frac{dR_{gr}}{dt} = k\left(\frac{1}{R_{gr}} - \frac{1}{R_{\max}}\right)$$

where k is a temperature dependent rate constant , R_{max} = $R_{max}(bu)$ the grain size at which growth stops. This burnup dependent quantity is introduced in order to account for the retarding effect of fission products on grain growth as burnup proceeds.

Most fission gas release models only account for the increase of the average diffusion distance when normal grain growth occurs. Some other models only take into consideration the sweeping effect, assuming either that the fractional release is proportional to the grain boundary velocity, or that the gas in the total fraction of grain volume swept by the grain boundaries is released. So they all fail to properly incorporate boundary motion into the intragranular diffusion equation and artificially separate the two aspects of grain growth on fission gas release. Only some stand-alone models have been proposed so far that account for both simultaneously by solving the diffusion equation in a sphere with a moving boundary (e.g. [37]).

For alleviating the fourth and fifth limitations of the Booth models, an intergranular module has to be introduced.

Intergranular behaviour
Three main different concepts are being applied. First of all, an intergranular model that does not model the kinetics at the grain boundaries directly. In a way the Booth model is a special case of this type, in that it considers gas atoms to be released as soon as they arrive at the grain boundary. The other models in this category consider gas arriving at the grain boundaries to precipitate straight away in grain boundary bubbles. An open tunnel network is assumed to be established along the grain boundaries once a so-called saturation value for the intergranular gas atom concentration (N_{max}) has been collected. In order to derive this saturation value, one assumes that
1. intergranular bubbles are lenticular, with θ being the dihedral angle between the grain boundary and the bubble surface (cf. Figure 13)
2. a mechanical equilibrium exists between the bubble gas pressure (p_{gas}), the surface tension (γ) and the hydrostatic pressure (σ_h) in the surrounding matrix: $p_{gas} = \dfrac{2\gamma}{\rho_{bl}} + \sigma_h$, where ρ_{bl} is the radius of curvature of the grain boundary bubble.
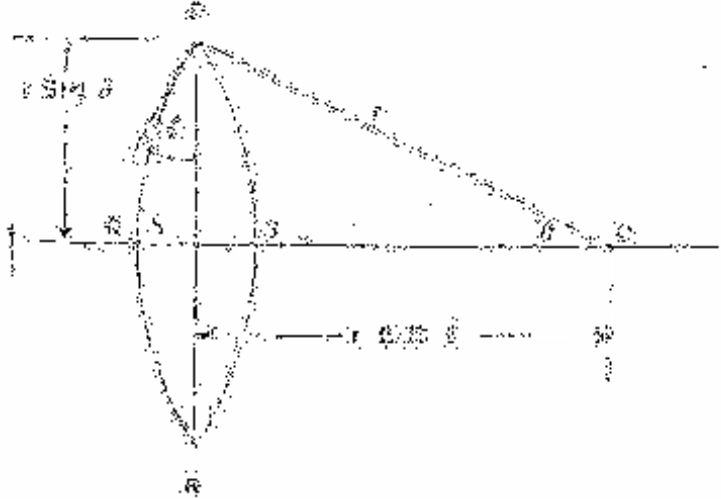3. a perfect gas law can be applied as equation-of-state

Figure 13: Schematic representation of a lenticular grain face bubble with radius of curvature *r*

Under those assumptions, the following expression is obtained for N_{max}:

$$N_{sat} = \frac{4\rho_{bl} f(\theta)}{3kT(\sin\theta)^2} \phi * \left(\frac{2\gamma}{\rho_{bl}} + \sigma_H\right)$$

where $f(\theta) = 1 - \frac{3}{2}\cos\theta + \frac{1}{2}(\cos\theta)^3$ and $\phi*$ stands for the fraction of the grain face surface occupied by the bubbles at interconnection. As soon as N_{max} is achieved, any excess gas atoms arriving at the grain boundaries are deemed released. It must be pointed out that no consensus has been reached at to what value should be applied for the hydrostatic stress. Often it is neglected, or a value is being used which is constant and uniform. Obviously this is a rough approximation.

In a second category of models, the intergranular kinetics is being considered directly. As such account is made of the reversible character of the tunnel establishment. The first model was proposed by White and Tucker [38]. They considered two parallel processes for release from the Booth sphere: intragranular diffusion and gaseous diffusion through tunnels along grain boundaries. To this end they solve two different diffusion equations in the equivalent Booth sphere. More recently, Koo et al. [39] proposed two different contributions for the *S/V* used to compute the equivalent Booth sphere radius. One contribution was attributed to macroscopic radial cracks in the pellet periphery, while the second contribution was ascribed to a fraction of the tunnel network along grain boundaries that was in contact with the open grain corner porosity (based on percolation theory in two dimensions). Recently, several other models have been proposed wherein the gaseous diffusion through the open tunnel network is being modelled according to Darcy's or Poisseuille's law in a tube (e.g., [24,40]). These models enable the effect of the hydrostatic pressure on the release kinetics to be accounted for. More recently White [41] went even further with the details and modelled the evolution of the bubble morphological relaxation through differential absorption/emission of vacancies, which is surface-curvature driven.

Nevertheless, these models are not yet implemented as standard models in fuel performance codes.

In a third category of models, a comprehensive list of mechanisms (cf. section 2.3.1) has been implemented in the form of a set of ordinary differential equations, i.e. the intra- and intergranular parts of the model are solved simultaneously (e.g. MARGARET [42]). These models were essentially produced to deal with fission product behaviour under severe-accident conditions. Up to now, only the FASTGRASS model of Rest [43] is being applied in the VICTORIA code [44].

Coupling intra and intergranular behaviour
In general, the intragranular and intergranular modules of a fission gas behaviour model are coupled in two directions. On one hand, the intragranular module provides the source term for the intergranular module. On the other hand, the intergranular module provides the boundary condition for the diffusion equation in the spherical grains and/or the supplementary source term near the grain boundary. In fact most models make use of the Booth approximations, i.e. they assume zero boundary conditions, meaning that the grain boundary is considered to be a perfect sink. Some models consider a finite segregation factor. In order to account for the resolution effect on grain boundary bubbles, three different approaches are being utilized. The first group considers a correction factor for the Booth flux, accounting for the fact that the resolution opposes the gaseous diffusion out of the grains. The second group of models applies a time-varying boundary condition that makes use of a time dependent flux balance. In the third and last group, a supplementary source term is defined in a fine layer adjacent to the grain face, either as a uniform source in a fine layer, or as a Dirac distribution at a given distance from the grain boundary. Mainly the first two approaches have been implemented in fuel performance codes.

Swelling
Theoretically speaking, the fission gas release and the fission gas swelling models should be closely related. In most codes, however, semi-empirical relations are being used for the gaseous swelling as a function of the temperature and burnup (e.g. MATPRO correlation [45,46]), or as an empirical function of the released fraction, for instance [47]:

$$\left(\frac{\Delta V}{V}\right)_{gaseousFP} = A\left(1 - \alpha_{FG}FGR - \alpha_{Cs}CSR\right)bu$$

where *A* is a constant for solid swelling, *FGR* the local fraction fission gas release from the grain, *CSR* the fractional release of the volatile fission products (Cs, I) from the grain, *bu* the local fuel burnup, α_{FG} = 0.37 and α_{cs} = 0.45. The empirical nature reflects the uncertainty pertaining to both the release and swelling models (in particular during power ramps at high burnup) as can also be inferred from the large variety of models presented above.

3. Advanced issues and future needs

3.1   Deterministic versus probabilistic analyses

In the introduction we have enumerated the various sources of uncertainties, and in the second section we have provided more details about the limitations of the models. In order to assess the technological effect of all sources of uncertainties there are various techniques that may be considered.

First of all, there are various so-called sensitivity methodologies, ranging from multiple runs with input data or model parameters being varied, up to a rigorous mathematical treatment based on perturbation theory. Apart from the numerical noise technique which is included in the TRANSURANUS code, the latter has never been applied to fuel rod modelling, probably because the mathematical effort would be too great to formulate all the non-linear phenomena in the form of basic differential equations. The numerical noise analysis allows the estimation of the standard deviation for instance of the centre line temperature within just one run. For this purpose, the most important parameters of the fuel rod (e.g. q' and λ) are varied slightly on a random basis in an interval, which is similar to introducing numerical noise. These changes of model parameters result in modifications of the resulting quantities, which enables the analysis of the sensitivity of the code with respect to its parameters. The computational effort is therefore identical with that of a deterministic run, but there is no information available about the effect between various uncertain parameters. Furthermore, changes of parameters may only produce modifications in the results that are smaller than the numerical accuracy. This can be overcome with an increased accuracy through a compiler option, along with an appropriate adaptation of the convergence limits.

A second category of probabilistic approaches is the response surface technique. This is based on a careful combination of parameters called the experimental design, such as the Latin hypercube sampling or the Taguchi design. Peck [48] tried this with the FRAP code. The main problem is that one has to decide in advance which parameter should be selected and how fine the variation of each parameter should be.

Finally, the Monte Carlo method is based on random sampling of all variables that are considered. It seems most attractive in view of its simplicity, but it entails high computational costs (factor 100-500), the knowledge about the distributions of the variables is rather limited, and it is unclear how much each parameter uncertainty contributes to the variation of the outcome. In order to reduce the computational costs, quasi-Monte Carlo methods may be applied. Instead of random sampling, quasi-random sampling sequences are recommended, which fill the space more uniformly than uncorrelated random numbers. They may be considered as a combination of the variations of parameters in response surface techniques with its experimental design and the standard Monte Carlo technique.

In Figure 14, a comparison is made between a deterministic and the two statistic analyses in the TRANSURANUS code. The points with the error bars indicate the mean value and the standard deviation of the centerline temperature at 4 distinct times according to a Monte Carlo analysis, whereas the dashed line indicates the standard deviation according to the numerical noise analysis. The comparison shows that the latter method, even though it is computationally equivalent to a single deterministic run, provides a similar approximation for the standard error of the center line temperature as the Monte Carlo technique in the case under consideration.
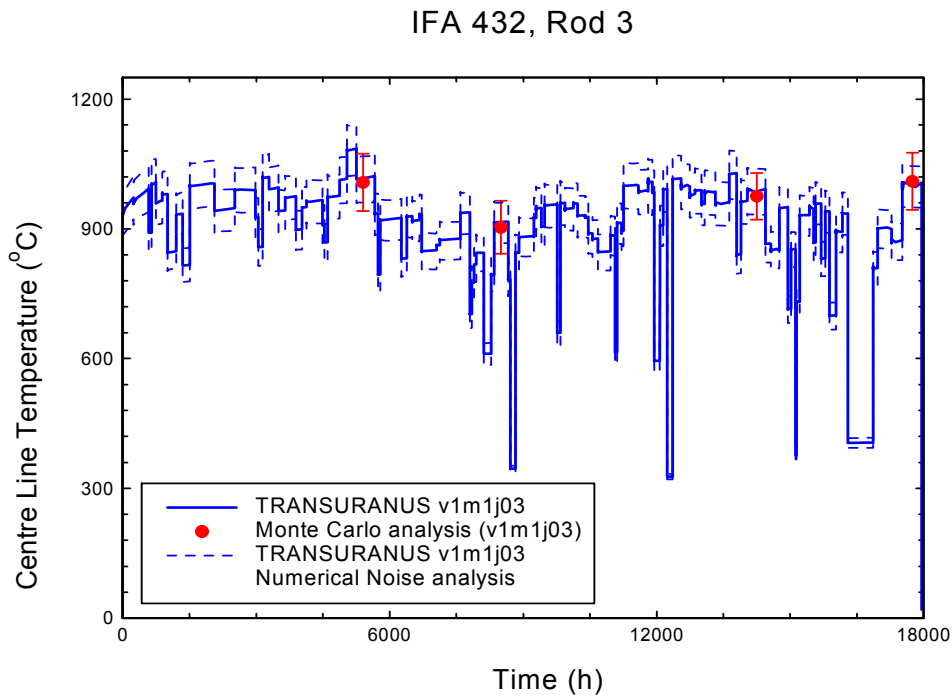

Figure 14: Comparision between a deterministic and two statistic analyses implemented in the TRANSURANUS code.

In Figure 15, a potential problem of a Monte Carlo calculation is illustrated. More precisely, when the standard deviations of the input variables and their distributions were chosen too high, the resulting temperatures cover a range from 850 -1260°C. It is not trivial to neglect results below a specific frequency.
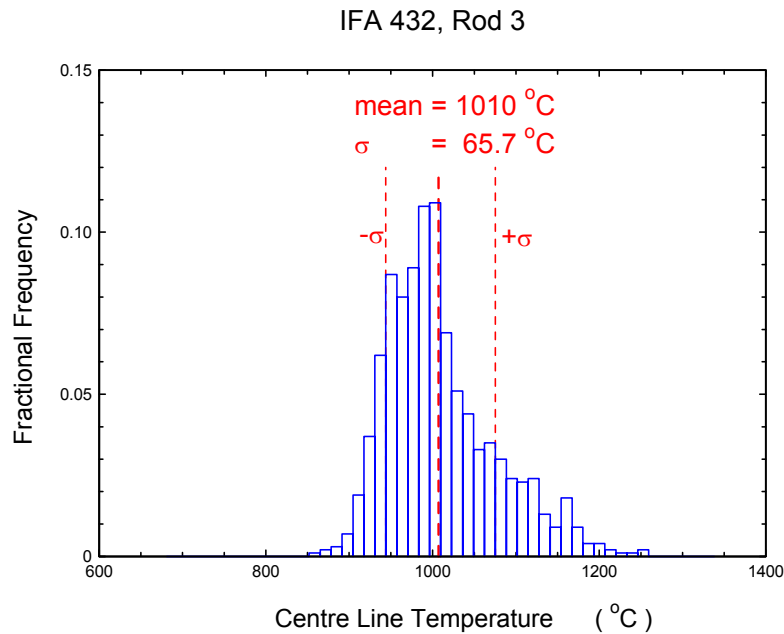
IFA 432, Rod 3

mean = 1010 ^{o}C
σ   = 65.7 ^{o}C

Figure 15: Fractional frequency of the centre line temperature predictions, when varying only three input parameters (q', h_{gap}, λ).

Despite the restrictions, applying a limited variation of some fabrication variable parameters in fuel rod performance calculations is being considered in Germany for two reasons. First of all, it is argued [49] that probabilistic calculations can replace a deterministic calculation with superimposed unfavourable tolerance limits on some fabrication parameters (worst case dataset) in fuel design calculations. The results obtained with the deterministic worst case calculation are said to be very conservative, with a degree of conservatism that would be difficult to quantify. Probabilistic calculations based on distributions on the other hand would allow the replacement of the worst case dataset by a dataset leading to results with a known, defined conservatism. The industry, of course, would like to reduce the margins in this way. Secondly, it has been observed that in some cases the deterministic conservative approach did in fact not predict the worst fuel performance as in a probabilistic approach. This of course, depends on the proper definition of the worst case on one hand, and on the limits of variation of the variable parameters in the Monte Carlo approach on the other hand.

3.2   High burnup fuel

3.2.1   Observations and importance of the high burnup structure

The resonance absorption of epi-thermal neutrons by U^{238} leads to the build up of Pu^{239} in the pellet periphery, after two successive β-decays. The high local burnup in combination with the low temperature leads to the formation of the high burnup structure (HBS), sometimes referred to as the "rim-effect" because of its appearance in the pellet rim (several 100 microns at a pellet burnup of 55 MWd/kgHM). The HBS is characterised by micron-sized pores

36

with a swelling contribution up to 15%, surrounded by small grains on the order of 100-300 nm with a very low but constant concentration of Xe around 0.25 w%. It starts in the pellet periphery when the local burnup exceeds a value of about 60 MWd/kgHM, and the local temperature remains below approximately 1000°C. It then progressively grows towards the pellet centre, as long as these two conditions are maintained.

The concomitant measurement of an increase of the fractional fission gas release in LWR fuel once the rod average burnup exceeded 45 MWd/kgHM, and the Xe depletion observed by means of electron probe microanalysis (EPMA) was first considered as an indication that there was a new release mechanism from the HBS. This was thought to be associated with the percolation through the large porosity that was collecting all the depleted Xe from the surrounding grains. In addition to such direct contribution from the HBS to the fractional release, the porosity formed in the pellet periphery was also assumed to constitute a thermal barrier. The resulting temperature increase would enhance the thermal release from the pellet interior, thereby providing an indirect contribution from the HBS to the observed increase in FGR. The thermal effect of the HBS was further supported by the observed thermal conductivity degradation with burnup.
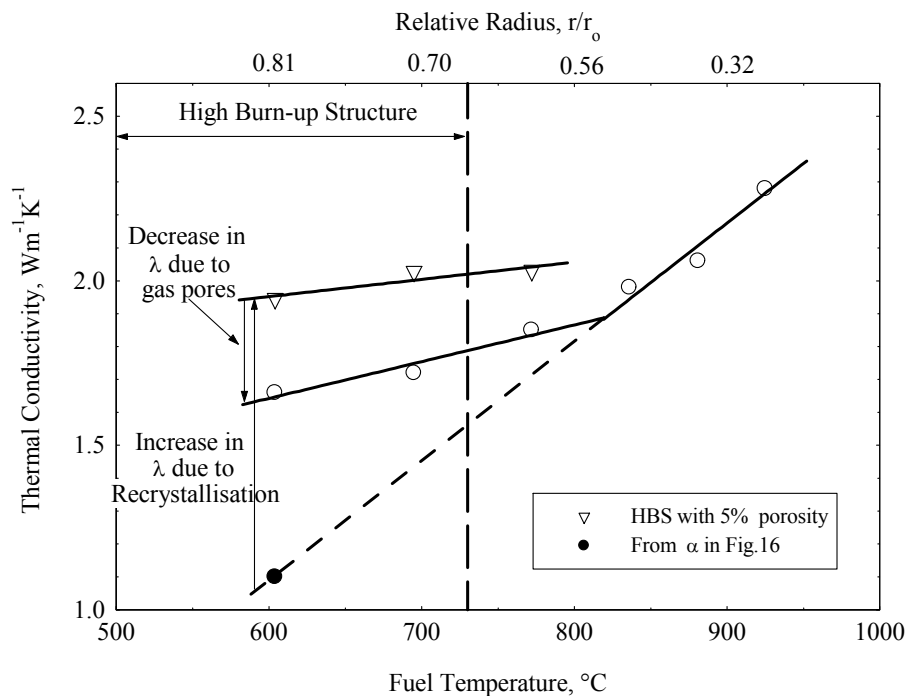

Figure 16: Thermal conductivity of the high burnup fuel at 217°C as a function of the local radial temperature during the last irradiation cycle. At $r/r_0 = 0.81$, where the local burnup was 90 MWd/kgHM, the local thermal conductivity of the fuel rod would have been 20% higher in the absence of gas pores. 5 % porosity is a hypothetical value equating to the porosity of the fresh fuel [50].

More recent observations [51], however, indicated that the HBS porosity is not interconnected, and that release from the HBS is too small to explain the increase of overall FGR measured during post irradiation examination on commercial fuel rods. Furthermore, new experimental evidence on thermal conductivity indicated that the Xe depletion in the matrix accompanying the

grain restructuring results in a restoration of the thermal conductivity, the effect of which is larger than the degradation due to the porosity buildup (Figure 16). Combining this with a measured decrease of the hardness along with an increase of the fracture toughness [52], the overall effect of the HBS on the fuel performance under normal operating conditions even seems beneficial rather than detrimental as originally feared.

The importance of the HBS during off-normal conditions, on the other hand still continues to be of concern. Indeed, the gas stored in the HBS porosity may contribute to the fuel dispersal, either during a sudden increase of the local temperature (e.g. during the first instants of a reactivity initiated accident or RIA), or during the cooling down when fuel micro-cracks form due to thermal stress relaxation.

3.2.2   *Modelling of the HBS*

In view of its implications on the fuel rod performance, the HBS has been the subject of many studies. Despite these efforts, no consensus could yet be obtained for several issues [53]. The most important is about a scenario describing the nucleation and growth of the HBS. This in turn is related to discussions about the driving force for the HBS formation (radiation damage and/or fission product accumulation), about the nucleation centres for the HBS nucleation (over-pressurised bubbles, grain boundaries, fabrication pores and dislocations or so-called recrystallisation nuclei), and about the parameters affecting the HBS formation and propagation (pellet-cladding contact pressure, initial grain size).

In fuel performance codes, the effect of the HBS on the heat transfer is generally included in a correlation describing the thermal conductivity degradation

$$\lambda = \frac{1}{A_0 + A_1 \cdot bu + B \cdot T}$$

and the porosity build up in the HBS as well as in an improved gap conductance in order to account for the bonding layer between the ceramic pellets and the metallic cladding. To this end, for example, the cladding and pellet roughness is empirically reduced above a certain burnup to account for the filling up by mainly zirconium oxide, which has a higher thermal conductivity than that of the mixture of He and Xe in the residual gap.

Thermal conductivity degradation of the fuel is sometimes considered to saturate

$$\lambda = \frac{\sqrt{\lambda_0}}{D\sqrt{bu}} \arctan\left(D\sqrt{bu}\sqrt{\lambda_0}\right) + \lambda_{el}$$

with λ_0 = *1/(A+BxT)* and *D* is a constant [54]. It can be shown that in the low burnup limit this expression tends to the classical form of λ_0. Occasionally

partial thermal conductivity restoration is even considered when the HBS is created. In this way account is made for the "cleaning" of the matrix from point defects and fission products, which relies on an empirical formulation of the lattice parameter variation [55]. The latter approach seems to be in line with the most recent experimental data shown in Figure 16.

The effect of the long irradiation time in the mechanical analysis is mostly accounted for in the cladding properties. The process of outer cladding corrosion liberates hydrogen from the water, and reduces the thickness of the cladding metallic wall. A fraction of that hydrogen, called the hydrogen pickup fraction is absorbed by the Zircaloy. This fraction depends on the composition and heat treatment of the cladding (and is usually introduced as a fitting constant). The hydrogen concentrates in the cold part of the cladding. As soon as the solubility limit is exceeded, it precipitates as brittle hydrides. When these hydrides are oriented normal to the cladding surface, the cladding strength is further reduced.

Reduction of the micro-hardness (Figure 17) and Young's modulus (cf. Figure 18) observed in high burnup fuel pellets is not yet included in the codes. This also holds for the bond between pellet and cladding, which improves the pellet-cladding interaction resistance since it is much softer than UO_2.
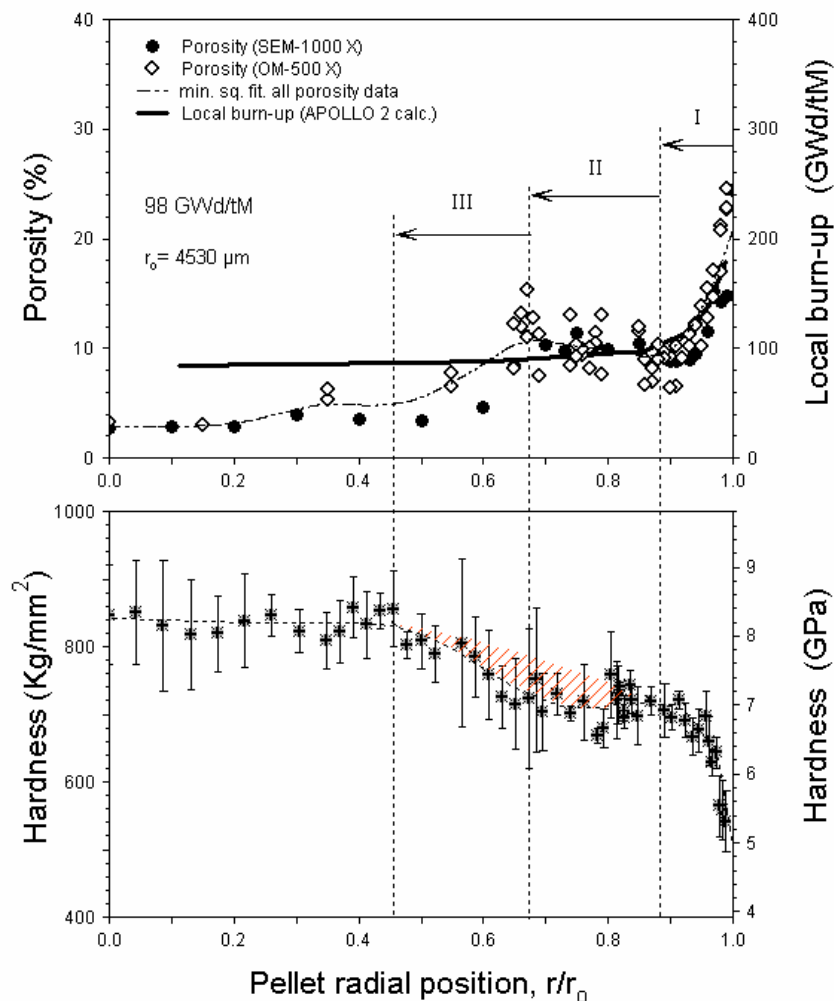

Figure 17: Experimental values for micro-hardness of irradiated UO$_2$ fuel with a burnup of 98 GWd/tHM [51]
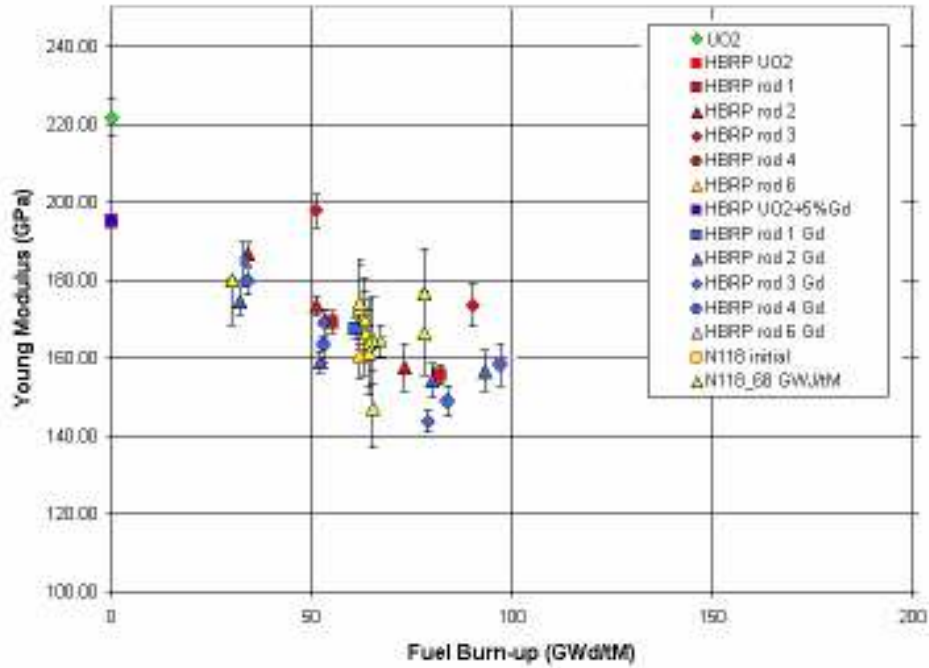
Figure 18: Experimental Young's modulus of irradiated LWR fuels as a function of burnup [56].

The HBS is associated to some extent with the radial power profile in the pellets. The resonance capture of epithermal neutrons in the peripheral regions of the pellets renders the application of neutron diffusion theory obsolete. In order to reproduce the stronger gradient in the pellet rim, fuel performance codes rely on empirically fitted functions reflecting the resonance capture, for instance in RAPID [57] or TUBRNP [58]. The latter solves the local differential equations for the uranium and plutonium isotopes:

$$\frac{dN_{235}(r)}{dbu} = -\sigma_{a,235}N_{235}(r)A,$$

$$\frac{dN_{238}(r)}{dbu} = -\sigma_{a,238}\overline{N}_{238}f(r)A,$$

$$\frac{dN_{239}(r)}{dbu} = -\sigma_{a,239}N_{239}(r)A + \sigma_{c,238}\overline{N}_{238}f(r)A,$$

$$\frac{dN_j(r)}{dbu} = -\sigma_{a,j}N_j(r)A + \sigma_{c,j-1}N_{j-1}(r)A.$$

The local concentration of ^{238}U, $N_{238}(r)$, is written as $\overline{N}_{238}f(r)$ where *f(r)* is a radial shape function with a normalisation factor defined by $\frac{2\int_{r_{in}}^{r_{out}} f(r)rdr}{r_{out}^2 - r_{in}^2} = 1,$, where r_{in} and r_{out} are the inner and outer fuel radii. The functions f(r), called

40

the radial shape function, is $f(r) = 1 + p_1 \exp\left(-p_2\left(r_{out} - r\right)^{p_3}\right)$. The constants p_1, p_2 and p_3 are fitted to EPMA data for each type of reactor.

The impact of the HBS on fission gas release is incorporated in various ways. The simplest way is based on an empirical threshold depending on the local burnup, and/or temperature and/or initial grain size. Others include the burnup as a parameter in the diffusion coefficient or the *S/V* value (for the Booth sphere radius), or in the grain boundary saturation value. Quantitative details of most models are not available in the open literature. In the START3 code [59] the grain size reduction observed is modelled in an empirical manner as a function of temperature and burnup. As the average distance for intragranular diffusion thereby reduces, an increased release fraction is predicted. Nevertheless, there is evidence that direct release from the HBS is small under normal operating conditions [51]. Apart from this general statement that the release is small, there is no consensus about the quantitative contribution from the HBS to the overall release under normal operating conditions. This is very well reflected in the large spread of fission gas release predictions at very high burnup for the codes involved in the FUMEX-II benchmark exercise organised recently by the IAEA (Figure 19).
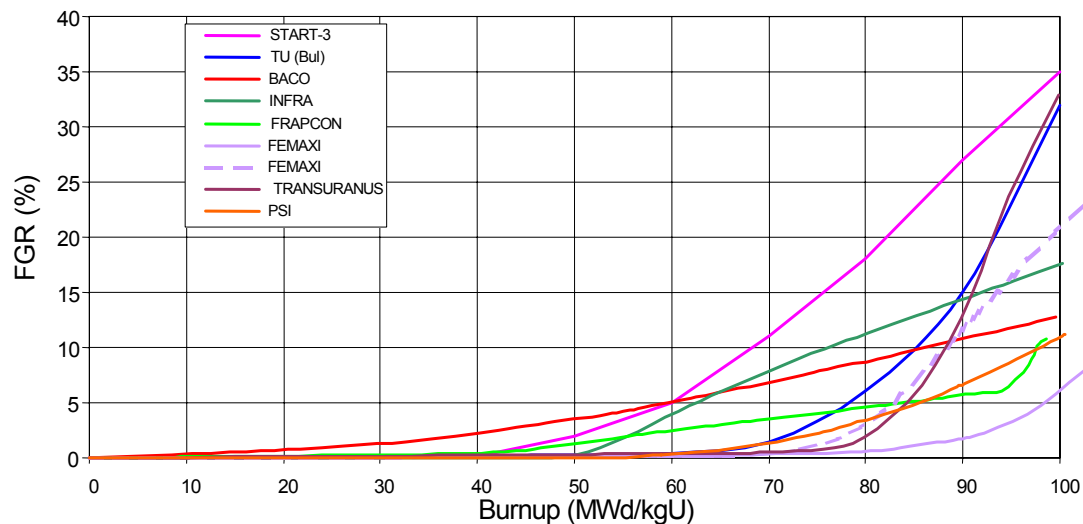

Figure 19: Cumulative fractional fission gas release predicted for a constant linear heat rate of 15 kW/m by various fuel performance codes involved in the FUMEX-II round robin exercise of the IAEA [60]

Under design basis accident conditions, the release models disregard the kinetics. Release is assumed to be instantaneous (provided that the gap is open) and comes from grain boundary cracking. The precise modelling of this relies on the modelling of the local conditions of temperature and stress, which is very difficult but hardly discussed in publications.

Finally, the swelling in the HBS is mostly modelled separately with a very simple linear or quadratic function of burnup (Figure 20). Also the width of the HBS structure is sometimes modelled empirically as a function of the burnup.
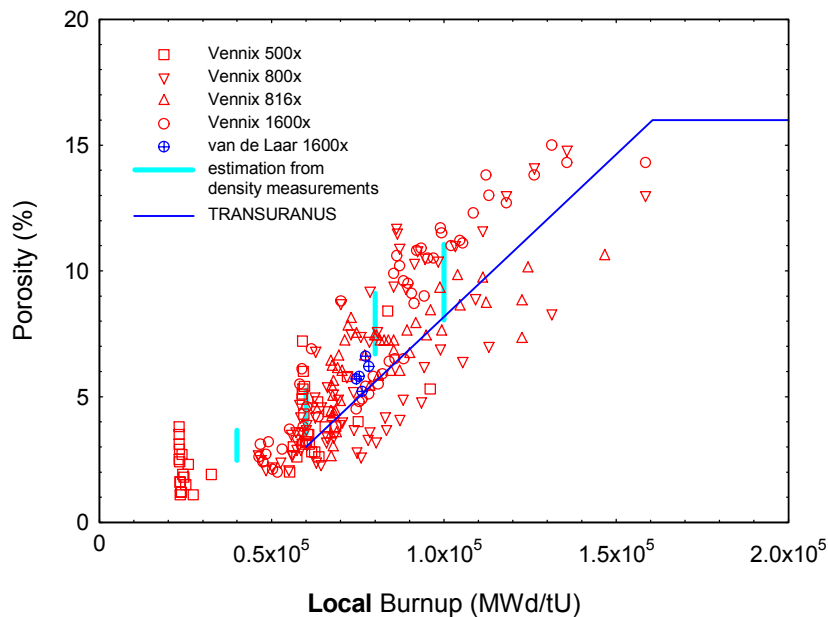
Figure 20: Porosity as a function of the local burnup for highly irradiated fuel, and the corresponding correlation adopted in the TRANSURANUS code [61].

3.3   Mixed oxide fuels

Since the plutonium concentration of MOX fuel in LWRs is low, its behaviour in a reactor is not very different from that of UO_2 fuel (more so because at end-of-life roughly 80% of the heat produced in UO_2 fuel comes from plutonium fissions). Consequently the fuel rod behaviour codes do not require fundamental modifications. The thermal properties such as melting temperature, thermal conductivity and expansion must be modified [62]. Also mechanical properties such as thermal creep and theoretical density require appropriate modifications.

In addition to material properties, a limited number of models must be adapted as well. The first obvious modification pertains to the neutronic model for computing the radial power profile and isotope production. In particular, the resonance capture in ^{240}Pu must be dealt with in a similar way as for ^{238}U, for instance with an empirical radial dependence, and dedicated effective cross-sections for MOX configurations in PWRs and BWRs must be used [63]. As such, one will be able to reproduce the larger flux depression in MOX at beginning of life (BOL), whereas at EOL the higher residual plutonium content at the centre will lead to higher local powers compared to those in UO_2 fuel.

Higher fission gas release at end of life is the only apparent problem mentioned for MOX fuel. It is mainly attributed to the higher linear powers at EOL, in combination with a lower thermal conductivity. This is corroborated by the similar threshold for thermal release measured in the Halden Boiling

Water reactor. According to these experiments, the Vitanza threshold (cf. sub-section 2.3.1) would apply to UO_2 and MOX fuel alike. Some experiments, however, indicate that the microstructure of some MOX fuel like MIMAS-MOX could also contribute to the higher release fractions. This has been ascribed to the heterogeneity at the microscopic scale, in particular to the Pu-enriched agglomerates characterised by a Pu-content around 25% and a size in the order of 50 microns. The burnup and fission product concentrations are therefore roughly three times higher in these agglomerates. Nevertheless, plutonium breeding in the UO_2 matrix surrounding the agglomerates together with fission product recoil tend to reduce the heterogeneity, in particular for agglomerates smaller than 30 microns, which can even "dissolve" in the UO_2 matrix.

In view of the particularities of fission gas release in MOX summarised above, three different modelling approaches are adopted: some codes do not modify anything since the use of existing uranium fuel FGR models for MOX fuel applications have been reported to give satisfactory results [64]. Some codes multiply the fission rate with a 'heterogeneity factor" to account for the higher athermal diffusion coefficient, or simply multiply the diffusion coefficient with a constant factor (~1.75). Some others have multiplied the FGR fraction based on the model for UO_2 with a so-called "heterogeneity factor" (~1.3). Finally there are stand-alone mechanistic models for FGR in MOX fuel wherein the evolution of the Pu-distribution in agglomerates and U-matrix is computed, the recoil from agglomerates is accounted for and/or the size-distribution of Pu-agglomerates is taken into account [65-67].

Another issue closely related to the FGR in MOX is the He production and release. Helium is generated in fuel matrices by alpha decay of transuranium nuclides and ternary fission, the former being the major source (cf. simplified nuclide chains in Figure 21).
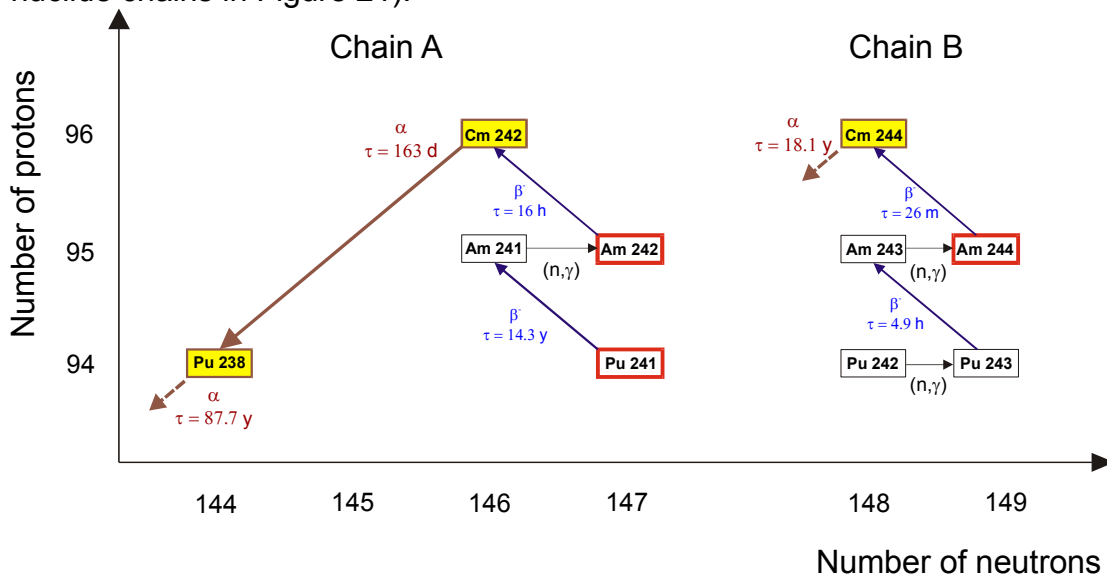

Figure 21: Simplified nuclide chains used for the approximative calculation of ^{4}He concentration in the TUBRNP model.

The He production is approximately 4-10 times higher in MOX in comparison with UO_2 fuel. Studies on He behaviour showed that its diffusion coefficient in

UO$_2$ is several orders of magnitude larger than that of noble gases. Nevertheless, its release from the fuel only occurs if its content is above the solubility limit. The latter strongly depends on temperature and He fill gas pressure [68], but is still being analysed for irradiated MOX. The solubility in fresh MOX fuel could explain why less release is observed in PWR rods (He fill gas pressure >20 bar) as shown in Figure 22, whereas significant release is observed in low pre-pressurised BWR MOX rods. This is why some codes do not consider the He release at all (in PWRs), while other codes use a simple (linear) correlation between the He release and fission gas release observed BWR MOX fuel (Figure 23).
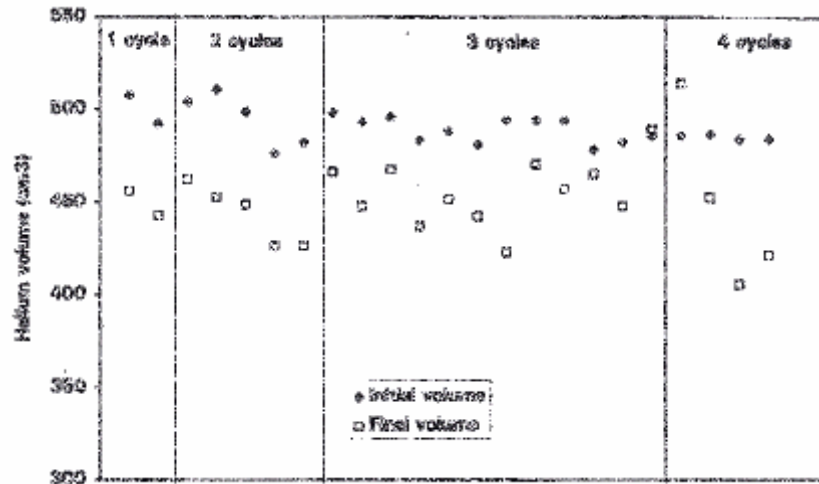

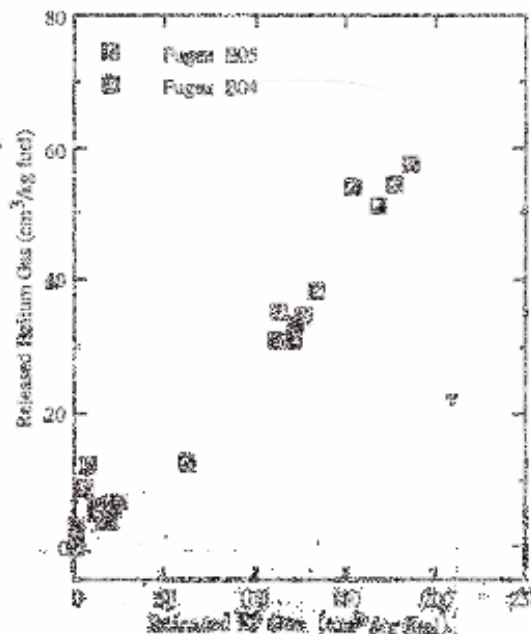**Figure 22: Helium balance in MOX PWR fuel rods, after [69]**

Figure 23: Comparison between He gas and fission gas release in BWR MOX fuel [70]

3.4 Multi-time-scale modelling

In the previous sections, the main models included in the fuel performance codes have been outlined. Every code contains semi-empirical correlations that are very valuable for technological applications. However, they are only valid within the confines of the parameters and irradiation conditions covered in the database on which they are developed. Extrapolating the models beyond their ranges of validation is not appropriate. In order to do so requires ideally, both more fundamental models, as well as the corresponding experimental data.

With the preparation of the next generation of nuclear reactors, advanced fuel types are being considered such as mixed nitrides and carbide fuels. The application of existing fuel performance codes to some of these materials requires a lot of new experiments. In view of complementing these experiments so as to guide the development and optimization of fuel processing, multi-time scale modelling is being proposed for new fuels [71]. In addition to the technological driving force, the approach also offers clear advantages from an academic point of view, as more knowledge is gained about the underlying basic mechanisms. It is therefore also being developed for the existing oxide fuels [72,73]. Starting with the application to existing oxides will also help to establish the right procedure for coupling the various techniques (cf. below), as much more experimental data are available for validating the multi-time-scale method. Originally, the method has first been developed for metals (e.g. [74-76]). As Illustrated in Figure 24, the method is hierarchical and based on passing information or parameters, starting from the electronic/atomic up to structural length and time scales. It should be underlined, that the building of a fuel performance code including the various techniques described below is quite unlikely despite the hardware evolution over the last decades. Some of the reasons are related to the limitations of the various techniques involved and will be underlined in the following sub-sections.
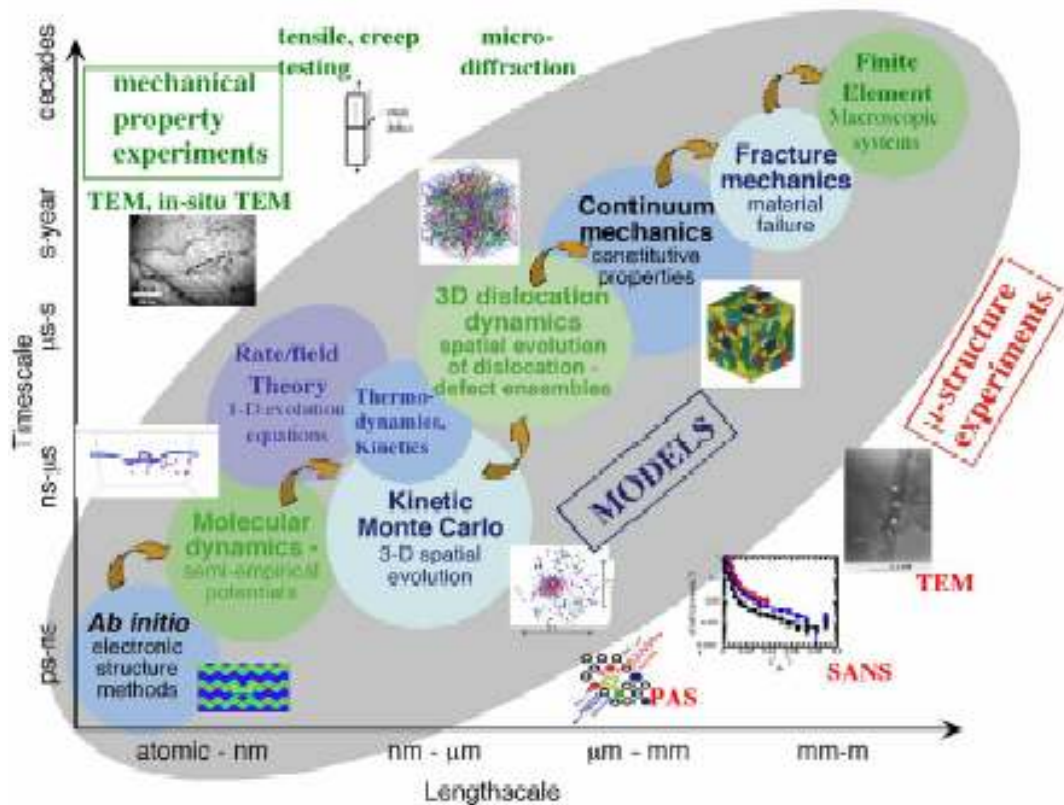
Figure 24: Illustration of an integrated experimental and computational approach to the multi-time-scale investigation of materials behaviour [74]. A number of microstructural characterisation techniques important for validating model predictions are also represented: Positron Annihilation Spectroscopy (PAS), Small Angle Neutron Scattering (SANS), Transmission Electron Microscopy (TEM).

3.4.1 Electronic and atomic scale modelling

At the electronic structure scale, first-principles or ab initio codes are being adopted. These tools rely on quantum mechanics and are solely based on the electronic/atomic structure of the materials. The ab initio codes enable quantitative properties of specific materials like the lattice constants, the structural stability (cohesive energy), and the elastic and bulk modulii to be obtained. These quantities, in turn, permits in principle, to extract the interatomic interaction potentials for the classical (Shell Model and Molecular Dynamics) modelling to be obtained. Simultaneously, such calculations give the electronic density distribution and energy bands (electronic structure) of materials, including the defect energy levels within the forbidden gap of the pure material. However, most reliable results from electronic structure calculations are obtained at 0 K. Comparison of these results with room or high temperature experimental results are therefore delicate. New methods that can provide results at finite temperatures are needed. Another drawback is the difficulty of calculating properties of mixtures and solutions for specific compositions. This is related to the relative small number of atoms involved in the calculation cell. Finally, to retrieve known materials properties and validate the calculations it is often necessary to use corrective parameters, used for instance in exchange-correlation functionals of Density Functional Theory.

Atomistic (e.g. Shell) models and simulations operate at nano-scales of the order of 5 Å, corresponding to inter-atomic distances. Although atomistic approaches are capable of capturing lower-scale properties, they do not incorporate quantum mechanics properties and only operate within the framework of classical mechanics. Inter-atomic potentials are often used for Molecular Dynamics (MD) simulations. Hundreds or even thousands of atoms are placed in the lattice sites associated with specific crystal structures and linked using the forces derived from inter-atomic potentials. The atoms are given initial velocities corresponding to the temperature under study and e.g. an incident particle gives energy (momentum) to a given host atom and then the structure is relaxed until minimum free energy is reached. Such simulations can describe times of the order of hundreds of pico-seconds, which is sufficient for calculations of equilibrium energy and for studies of defect formation and migration, as well as dislocation propagation. However, the simulation times are not long enough to address phenomena such as diffusion or cascade effects during irradiation.

To allow for longer simulation times, MD could be coupled with Monte Carlo (MC) methods. During MC calculations, the solution space is sampled and only points that satisfy certain criteria are accepted. Another option is to use temperature accelerated dynamics (TAD). TAD is based upon molecular dynamics and increases the rate of events by artificially increasing the temperature. The behaviour at the temperature of interest is determined by a mapping technique. Atomistic methods rely on good inter-atomic potentials. Many-body effects and 3-atom interactions, accounted for in semi-empirical potentials such as the modified embedded atom method, have been included in potentials for metals and alloys but not for actinide based ceramics. The main reason is the very difficult process of incorporating charge transfer between atoms. The most reliable models for actinide based ceramics involve pair-potentials.

Until now, most calculations for radiation defects and fission gas diffusion were performed only for UO_2 fuel using the empirical potentials (Shell Model, SM) [77-79]. It is important to check SM calculations by *ab initio* modelling, in order to confirm that the chemical bond covalency is properly taken into account via empirical parameters, and if there is not considerable charge redistribution at the saddle point of defect (Xe atom) migration hops. The MD simulations were performed so far only for preliminary understanding of basics of the radiation damage of simple ionic oxides, like MgO, as well as for a first attempt to evaluate thermal properties of UO_2 and MOX [80-82].

Ab initio calculations of UO_2 and point defects therein were started very recently [73] using plane-wave Density Functional Theory (DFT) calculations with pseudopotentials. This approach was extended for the modelling of some fission products (Kr, I, Cs, Sr and He) [72]. The main problem of these calculations is the inability of the DFT approach to reproduce the insulating nature of the UO_2, and thus its inability to study charged defects. Another important shortcoming is the lack of analysis of the chemical bonding covalency, which is a general problem for all plane-wave methods.

3.4.2 Mesoscale and continuum modelling

Modelling at the mesoscopic scale is of interest for instance in understanding the evolution and role of dislocations in nuclear fuels. In nuclear fuels, dislocations are assumed to play also an important role in the formation of the HBS. In order to clarify the conditions of the restructuring observed in the HBS of nuclear fuels, it is of primary importance to be able to describe the interaction between dislocations, and subsequently between dislocations and point defects as well as pores or precipitates observed. Given the various types of dislocations (edge, screw and mixed types of dislocations), as well as the variety of configurations of dislocation arrays observed, a general method is required to describe the stress and associated energy. Hitherto, the methodology of Kröner [83] has been applied to develop a tool with which stress distributions associated with all types of dislocation configurations can be analyzed [84]. Extension of the tool to include interactions with precipitates and pores are necessary for the theoretical analysis of the micro-polygonisation of the restructured area in nuclear fuels.

In the section on mechanical analysis (section 2.2), it was already underlined that 2D and 3D mechanical calculations are mandatory for a correct analysis of the mechanical interaction between deformed pellets or their fragments with the cladding. The 1.5D description in fuel performance code allows for modelling of all the phenomena involved in case of a ramp test, but the 3D description enables a local description of the stress and strain fields on the scale of geometrical singularities of the pellet, as illustrated in Figure 25. The numerical scheme in a 3D analysis typically takes into account thermal and mechanical coupling induced by the heat exchange evolution in the pellet-cladding gap [2,22]. Elastic and inelastic strains accumulated in the cladding are computed simultaneously at every time step. As a result, this scheme allows also computation of severe thermal transients. Additionally, a Coulomb friction model at pellet cladding interface has been implemented [2]. Associated with the initial pellet cracking, it shows stress and inelastic strain concentration at the inter-pellet level in front of the fuel radial cracks. This result is consistent with experimental observation of a Pellet Cladding Interaction/Stress Corrosion Cracking (PCI/SCC) cladding failure initiating in this area during power transients. Two sets of boundary conditions imposed on the modelled fuel rod segment allow closing up the unknown load resulting from the friction in the remaining unmodelled part. Despite its clear advantages, 3D calculations are still expensive in terms of calculation time. Furthermore, they are quite sensitive to the boundary conditions as well as the friction coefficients (for which a large range of values are being used). Finally, the stochastic nature of the cracking offsets the advantages and justifies the use of 1.5D modelling in fuel performance codes.
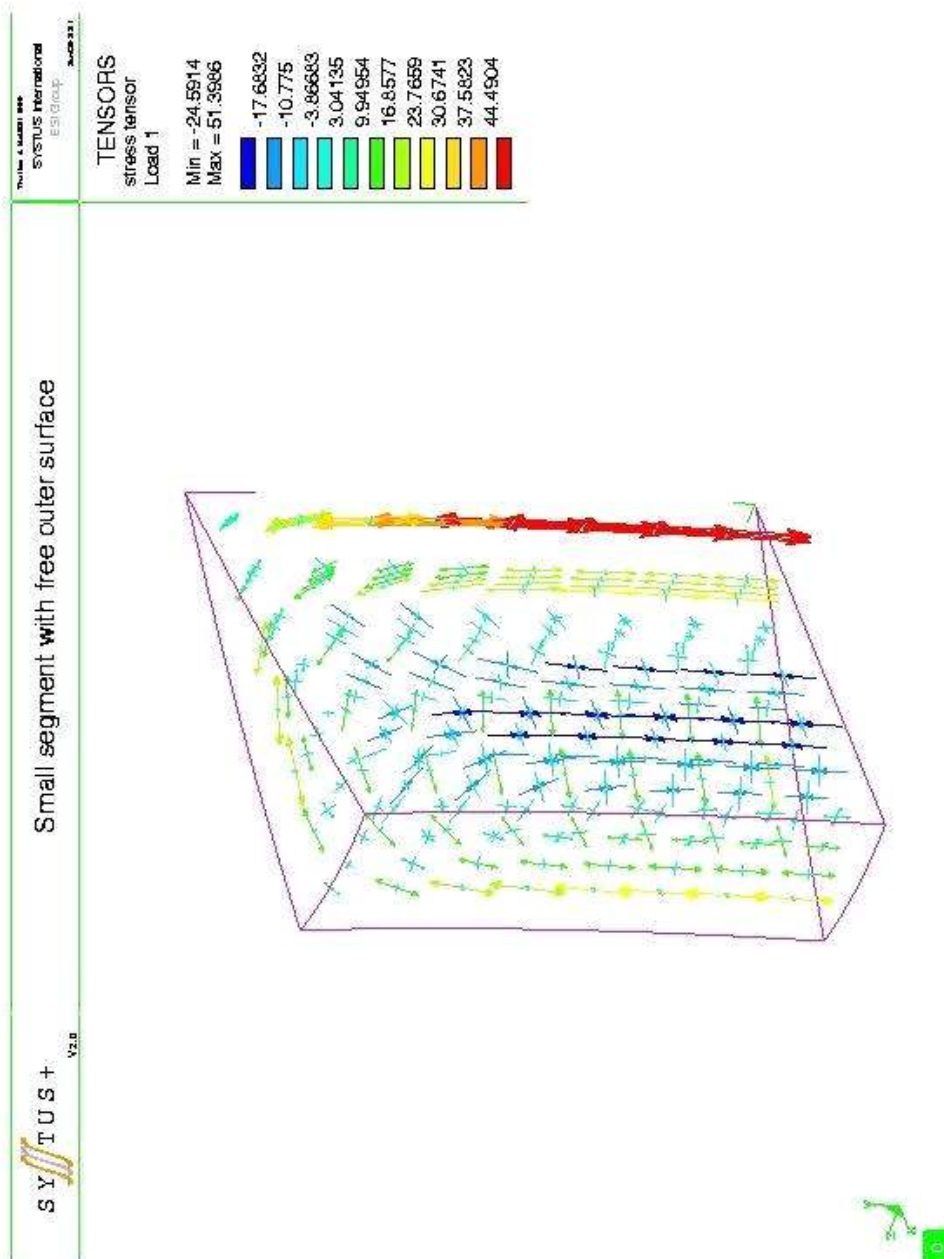
Figure 25: Stress tensor obtained with 3D FEM thermo-elastic calculation in a small fuel segment (height: 6.5 mm, radius: 5.3 mm, angle = 22.5 degr.) and subject to a parabolic temperature gradient (Tsurface = 400^{0}C , Tcenter = 1000^{0}C) [22].

4. Summary and conclusions

The modelling of nuclear fuel behaviour involves many phenomena and disciplines ranging from chemistry, nuclear and solid state physics, metallurgy, ceramics, and applied mechanics. The strong interrelationship between these disciplines, as well as the non-linearity of many of the processes involved calls for the development of computer codes describing the general fuel behaviour. After several decades of modelling, the fuel behaviour codes have become standard tools for safety authorities, fuel designers and nuclear fuel researchers. The various benchmarks for fuel rod performance codes organised by the IAEA [60] revealed that in general under normal operating conditions

- temperatures can be predicted with a relative error of the order to 10%;
- the clad elongation as well as the cladding diametrical deformation are predicted with a relative error of about 30% (although based on less data);
- the ratio of predicted to measured values for fission gas release is generally within a factor of 2.

Most difficulties stem from

- uncertainties in input values (fabrication and irradiation parameters);
- the stochastic nature of pellet cracking, and its consequences on the thermal (uncertainty on the gap size, especially at beginning-of-life) as well as on the mechanical analysis (validity of compatibility and constitutive equations). In addition, crack-healing is difficult to model properly;
- a lack of direct measurements (e.g. stresses or parameters such as diffusion coefficients and resolution rate coefficients) or large scatter in the experimental data;
- a limited set of experimental data available in the open literature for new materials that are being introduced for reaching higher discharge burnups (e.g. new cladding material properties).

It should be underlined that some specific fuel performance codes (typically developed by fuel vendors) have been fine-tuned with a larger data base but for a particular type of fuel and therefore provide more accurate predictions for this type of fuel.

In view of the tendency to increase the discharge burnup of fuel rods, modifications have been made or still need to be implemented. In particular for the thermal conductivity, recent measurements revealed that the high burnp structure leads to a recovery (as point defects and fission products are removed from the fuel matrix) which is more important than the impedance to the heat flow resulting from the concomitant porosity build up. In parallel, the bonding layer between the fuel and the cladding at these burnup levels eliminates progressively the effect of surface roughness on the heat transfer in the gap.

With respect to the mechanical properties, various experimental techniques indicate a softening of the fuel when the high burnup structure is established.

As far as the fission gas behaviour is concerned, there is a consensus that most fission gas remains in the HBS (approximately 90%), whereas earlier it was believed to be responsible for the observed increase in fission gas release beyond average burnup levels of 50 MWd/kgHM. Despite the relatively benign effects of the HBS on the thermo-mechanical behaviour of the fuel rod under normal operting conditions, the HBS still requires attention for modelling the transient behaviour of nuclear fuel. In the event of a Reactivity Initiated Accident, for example, it is important to know how much gas resides in porosity and could contribute to the rapid mechanical loading of the cladding. The quantification of the gas distribution at high burnup still requires more experimental efforts.

Modelling the behaviour of MOX fuel for LWRs has also become an routine task in some specific countries as it became a mature industrial product. Generlly, the fission gas release fraction at end-of-life is higher in comparison with that of UO_2 fuel. The difference in power history and the lower thermal conductivity of MOX have been identified to be the main causes, although research is still ongoing to assess the role of the heterogeneous microstructure in (MIcronized MASter blend, or MIMAS-type) MOX.

The mechanistic models for FGR for MOX available in the open literature do not account for the evolved microstructure, which apart from the Pu-rich agglomerates and U-rich matrix may also contain a Pu-rich coating layer at grain boundaries.

With respect to helium, the fractional release observed in MOX fuel rods loaded in BWRs is generally taken to be proportional with the FGR fraction. In contrast, the absence of He release observed in PWR MOX has been ascribed to the higher He solubility due to the elevated fill gas pressure. With the potential inclusion of higher amounts of He-generating minor actinides in MOX fuel, and the long storage times of spent fuel, the issue of He release will gain importance in the codes. Nevertheless, more experimental data are needed in the open literature for MOX fuel.

In order to complement the time-consuming and costly experiments for developing and optimizing advanced fuels for the next generation of reactors, multi-time-scale modelling is being launched across the globe. Yet, despite promising results for the behaviour of fission products in UO_2, and a better understanding of the basic phenomena, it is still too ambitious to conceive a fuel performance code based solely on fundamental computations. There are limitations to each individual technique in terms of temperature range, space – and time-scale, in addition to the stochastic nature of several phenomena (e.g. fuel cracking) or the strong relationship between various phenomena entailing high non-linearities.

Until recently fuel performance codes were either developed for simulating the fuel rod behaviour under normal operating conditions and mild transients, or for simulating accident behaviour. At present there is a tendency to widen the scope of both types of codes so as to simulate the fuel rod behaviour under all

conditions with a single code in a more consistent manner. A good example is the TRANSURANUS code, the structure of which has been conceived correspondingly right from the start.

Finally, it is important that all fuel performance codes will be further benchmarked with peer-reviewed experimental data, such as those proposed in the frame of international benchmarks organised by the OECD/NEA and the IAEA.

Acknowledgements

Appendix 1: List of some codes used for modelling the LWR fuel rod behaviour

This list is not intended to be comprehensive. Some of the well-known codes are:

COMETHE	N. Hoppe, M. Billaux, J. van Vliet, S. Shihab, "COMETHE version 4D release 021 (4.4-021), Vol. 1, general description", Belgonucleaire report BN-9409844/220 A, April 1995
COPERNIC[1]	E. Bonnaud, C. Bernard, E. Van Schel, "COPERNIC: A state-of-the-art fuel rod performance code", Trans. Am. Nucl. Soc., Vol. 77 ; Dec. 1997
ENIGMA	W.J. Kilgour, J.A. Turnbull, R.J. White, A.J. Bull, P.A. Jackson, I.D. Palmer, "Capabilities and validation of the ENIGMA fuel performance code", Proc. ENS Meeting on LWR Fuel Performance, Avignon, France, 1992
FALCON, FREY	J. Rashid, R. Montgomery, S. Yagnik, R. Yang, "Behavioral modeling of LWR fuel as represented in the FALCON code", Proc. Workshop on Materials Modelling and Simulations for Nuclear Fuel, New Orleans, USA, Nov. 2003
FEMAXI	M. Suzuki, "Light water reactor fuel analysis code FEMAXI-V(Ver.1)", JAERI-Data/Code 2000-030, July 2000
FRAPCON	G.A. Berna, C.E. Beyer, K.L. Davis, D.D. Lanning, "FRAPCON-3: A computer code for the calculation of steady-state, thermal-mechanical behaviour of oxide fuel rods for high burnup", NUREG/CR-6534, PNNL-11513, Dec. 1997
METEOR[1]	C. Struzik, M. Moyen, J. Piron, "High burnup modelling of UO_2 and MOX fuel with METEOR/TRANSURANUS Version 1.5", Proc. Int. Top. Meet. on LWR Fuel Performance, Portland, Oregon, USA, March 1997

PIN-micro	F. Pazdera, P. Strijov, M. Valach, et al., "User's guides for the computer code PIN-micro", UJV 9512-T, Rez, Nov. 1991
START	Y.K. Bibilashvili, A.V. Medvedev, G.A. Khostov, S.M. Bogatyr, L.V. Korystine, "Development of the fission gas behaviour model in the START-3 code and its experimental support", Proc. Int. Sem. On Fission Gas Behaviour in Water Reactor Fuels, Cadarache, France, Sep. 2000
TRANSURANUS	K. Lassmann, "The TRANSURANUS Code – past, present and future", Review article, ITU Activity Report 2001 – EUR 20252, ISBN 92-894-3639-5 (2001)

[1]based on TRANSURANUS

References

[1]   S. K. Yagnik, "Overview of EPRI Fuel Peformance Code FALCON", Seminar Proceedings, Nuclear Science, Cadarache, France, 3-6 March, 1998, pp. 267-272.

[2]   F. Bentejac, N. Hourdequin, "TOUTATIS, an application of the CAST3M finite element code for PCI three-dimensional modelling", International Seminar on Pellet-Clad Interaction in Water Reactor Fuels, Aix-en-Provence, France, 9-11 March, 2004.

[3]   D. R. Olander, "Fundamental aspects of nuclear reactor fuel elements", 1976, TID-26711-P1.

[4]   H. Bailly, D. Ménessier, C. Prunier, "The nuclear fuel of pressurized water reactors and fast reactors", Lavoisier Publishing, 1999, ISBN CEA 2-7272-0198-2.

[5]   K. Lassmann, P. Van Uffelen, "The Structure of Fuel Rod Codes", Publications Office, JRC Publications, Report EUR 21400 EN, European Commission, 2004.

[6]   K. Lassmann, F. Hohlefeld, "Überarbeitung des URGAP Modells zur Berechnung des Wärmeübergangs zwischen Brennstoff und Hülle", Report EUR 10756 DE, European Commission, 1986.

[7]   K. Lassmann, F. Hohlefeld, "The Revised URGAP-Model to Describe the GAP Conductance Between Fuel and Cladding", Nucl. Eng. Des., Vol. 103, pp. 215-221, 1987.

[8]   K. Lassmann, C. T. Walker, J. van de Laar, "Extension of the TRANSURANUS Burnup Model to Heavy Water Reactor Conditions", J. Nucl. Mater., Vol. 255, pp. 222-233, 1998.

[9]   K. Lassmann, "The Structure of Fuel Element Codes", Nucl. Eng. Des., Vol. 57, No. 1, pp. 17-39, April 1980.

[10]   K. Lassmann, "A Fast and Simple Iteration Scheme for the Temperature Calculation in a Fuel Rod", Nucl. Eng. Des., Vol. 103, pp. 211-214, 1987.

[11]   K. Lassmann, "TRANSURANUS: A Fuel Rod Analysis Code Ready For Use", J. Nucl. Mater., Vol. 188, pp. 295-302, 1992.

[12]   H. Assmann, H. Stehle, "Thermal and in-reactor densification of UO_2 mechanisms and experiments", Nucl. Eng. Des., Vol. 48, pp. 49-67, 1978.

[13]   H. C. Suk, W. Wang, B. G. Kim, K. S. Kim, Y. H. Heo, "Improvement of ELESIM-CANDU fuel performance analysis code", Tech. Com. Meeting on fission gas release and fuel chemistry related to extended burnup, Pembroke, Ontario, Canada, April, 1992, pp. 193-201, IAEA-TECDOC-697.

[14]   P. A. Jackson, J. A. Turnbull, R. J. White, "A description of the ENIGMA fuel performance code", Report IAEA-TECDOC-697, pp. 28-38, 1989.

[15]   M. E. Cunningham, C. E. Beyer, P. G. Medvedev, G. A. Berna, H. Scott, "FRAPTAN: a computer code for the transient analysis of oxide fuel rods", Report NUREG/CR-6739, Vol.1, PNNL-13576, August 2001.

[16]   M. Suzuki, "Light Water Reactor Fuel Analysis Code FEMAXI-V(Ver.1)", JAERI-Data/Code 2000-030, July 2000.

[17] P. Garcia, C. Struzik, M. Agard, V. Louche, "Mono-dimensional mechanical modelling of fuel rods under normal and off-normal operating conditions", Nucl. Eng. Des., Vol. 216, pp. 183-201, 2002.

[18] A. R. Massih, L. O. Jernkvist, "Mechanics and PCMI", Chapter 6 in lecture notes of the OECD - HRP Summer schoolon fuel behaviour modelling, Halden, Norway, 31 August - 3 September, 2004.

[19] M. Oguma, "Cracking and Relocation Behavior of Nuclear Fuel Pellets During Rise to Power", Nucl. Eng. Des., Vol. 76, pp. 35-45, 1983.

[20] G. A. Berna, C. E. Beyer, K. L. Davis, D. D. Lanning, "FRAPCON-3: A computer code for the Calculation of Steady-State, Thermal-Mechanical Behaviour of Oxide Fuel Rods for High Burnup", Report NUREG/CR-6534, PNNL-11513, December 1997.

[21] K. Lassmann, A. Schubert, P. Van Uffelen, J. van de Laar, "TRANSURANUS Handbook", 2005.

[22] P. Van Uffelen, M. Sheindlin, V. Rondinella, C. Ronchi, "On the Relations between the Fission Gas Behaviour and the Pellet-Cladding Mechanical Interaction in LWR Fuel Rods", Pellet-Clad Interaction in Water Reactor Fuels (PCI-2004), CEA Cadarache/DEN/DEC, Aix en Provence, France, 9-11 March, 2004.

[23] V. Z. Jankus, R. W. Weeks, "LIFE-II - a computer analysis of fast-reactor-fuel-element behaviour as a function of reactor operating history", Nucl. Eng. Des., Vol. 18, pp. 83-96, 1972.

[24] P. Van Uffelen, Contribution to the Modelling of Fission Gas Release in Light Water Reactor Fuel, PhD Thesis, Nuclear engineering, University of Liege, 2002.

[25] R. W. Grimes, "Simulating the behaviour of inert gases in UO_2", in: "Fundamental aspects of inert gases in solids", Vol. 279, NATO Advanced Science Institute, Series B, Plenum Press, 1991 pp. 415-429.

[26] J. A. Turnbull, C. A. Friskney, J. R. Findlay, F. A. Johnson, A. J. Walter, "The diffusion coefficients of gaseous and volatile species during the irradiation of uranium oxide", J. Nucl. Mater., Vol. 107, pp. 168-184, 1982.

[27] D. R. Olander, P. Van Uffelen, "On the role of grain boundary diffusion in fission gas release", J. Nucl. Mater., Vol. 288, pp. 137-147, 2001.

[28] H. Matzke, "Gas release mechanisms in UO_2 - a critical overview", Radiation Effects, Vol. 53, pp. 219-242, 1980.

[29] C. Vitanza, U. Graziani, N. T. Fordestrommen, K. O. Vilpponen, "Fission Gas Release from in-pile Measurements", Report HPR-221.10, OECD Halden Reactor Project, 1978.

[30] C. Vitanza, E. Kolstad, C. Graziani, "Fission gas release from UO_2 pellet at high burnup", American Nuclear Society, Topical Meeting on Light Water Reactor Fuel Performance, Portland, Oregon, May, 1979.

[31] A. H. Booth, "A method of calculating fission gas diffusion from UO_2 fuel and its application to the x-2-f loop test", Report CRDC-721, AECL, Chalk River, Ontario, Canada, 1957.

[32] A. H. Booth, "A suggested method for calculating the diffusion of radioactive rare gas fission products from UO2 elements and a discussion of proposed in-reactor experiments that may be used to test its validity", Report DCl-27, AECL, Chalk River, Ontario, Canada, 1957.

[33] K. Lassmann, H. Benk, "Numerical algorithms for intragranular fission gas release", J. Nucl. Mater., Vol. 280, pp. 127-135, 2000.

[34] M. V. Speight, "A calculation on the migration of fission gas in material exhibiting precipitation and re-solution of gas atoms under irradiation", Nucl. Sci. Eng., Vol. 37, pp. 180-185, 1969.

[35] P. Lösönen, "On the behaviour of intragranular fission gas in UO_2 fuel", J. Nucl. Mater., Vol. 280, pp. 56-72, 2000.

[36] J. B. Ainscough, B. W. Oldfield, J. O. Ware, "Isothermal grain growth kinetics in sintered UO_2 pellets", J. Nucl. Mater., Vol. 49, pp. 117-128, 1973.

[37] K. Forsberg, A. R. Massih, "Theory of fission gas release during grain growth", Structural Mechanics in Reactor Technology (SMiRT16), Washington DC, Aug 12-17, 2001.

[38] R. J. White, M. O. Tucker, "A new fission gas release model", J. Nucl. Mater., Vol. 118, pp. 1-38, 1983.

[39] Y. H. Koo, D. S. Sohn, Y. K. Yoon, "An analysis method for the fuel rod gap inventory of unstable fission products during steady-state operation", J. Nucl. Mater., Vol. 209, pp. 62-78, 1994.

[40] T. Kogai, "Modelling of fission gas release and gaseous swelling of light water reactor fuels", J. Nucl. Mater., Vol. 244, pp. 131-140, 1997.

[41] R. J. White, "The development of grain-face porosity in irradiated oxide fuel", J. Nucl. Mater., Vol. 325, pp. 61-77, 2004.

[42] L. Noirot, "MARGARET: An advanced mechanistic model for fission gas behaviour in nuclear fuel", Inter. Topical Meeting on Light Water Reactor Fuel Performance, ANS, Kyoto, Japan, Oct 2-5, 2005.

[43] J. Rest, S. A. Zawadski, "FASTGRASS: A mechanistic model for the prediction of Xe, I, Cs, Te, Ba and Sr release from nuclear fuel under normal and sever-accident conditions", Report NUREG/CR-5840, ANL-92/3, April 1992.

[44] D. R. Olander, V. Mubayi, "Review of the materials-chemistry models in the VICTORIA code", J. Nucl. Mater., Vol. 270, 1-2, pp. 1-10, April 1999.

[45] MATPRO library, Report NUREG/CR-5273, EGG-2555, 1990

[46] "MATPRO-Version 11 (Revision 2), A handbook of material properties for use in the analysis of light water reactor fuel rod behaviour", Report NUREG/CR-0497, TREE-1280, Rev. 2, 1981.

[47] M. R. Billaux, "Fuels performance, limits, operational and safety issues", Lecture notes at Frederic Joliot-Otto Hahn 2005 summer school, Karlsruhe, Germany, 24 August - 2 September, 2005.

[48] S. O. Peck, "Automated uncertainty analysis methods in the FRAP computer codes", IAEA Specialist's Meeting on Fuel Element Performance Computer Modelling, Blackpool, U.K., 1980.

[49] L. Heins, H. Groß, K. Nissen, F. Wunderlich, "Statistical analysis of QC data and estimation of fuel rod behaviour", J. Nucl. Mater., Vol. 178, p. 287, 1991.

[50] C. T. Walker, D. Staicu, M. Sheindlin, D. Papaioannou, W. Goll, F. Sontheimer, "On the thermal conductivity of UO_2 nuclear fuel at a high burn-up of around 100 MWd/kgHM", J. Nucl. Mater., Vol. 350, pp. 19-39, 2006.

[51]   J. Spino, A. D. Stalios, H. Santa Cruz, D. Baron, "Stereological evolution of the rim structure in PWR-fuels at prolonged irradiation: Dependencies with burn-up and temperature", J. Nucl. Mater., Vol. 354, pp. 66-84, 2006.

[52]   "Annual report of the Institute for Transuranium Elements", Report EUR 22105 EN, 2005.

[53]   P. Van Uffelen, J. Jonnet, C. Ronchi, "Open Questions related to the high burnup structure in nuclear fuels", Proc. of Workshop Materials Models and Simulations for Nuclear Fuels, No 18-19, Washington, DC, USA, 2004.

[54]   F. Sontheimer, H. Landskron, M. R. Billaux, "A fuel thermal conductivity correlation based on the latest experimental results", Proc. Seminar on Thermal Performance of High Burn-up LWR fuel, Cadarache, France, 3-6 March, 1998, p. 119.

[55]   D. Baron, "About the Modelling of fuel thermal conductivity degradation at high-burnup accounting for recovering process with temperature", Proc. Seminar on Thermal Performance of High Burn-up LWR fuel, Cadarache, France, 3-6 March, 1998, pp. 129-143.

[56]   D. Baron, R. Masson, J. Gatt, J. Spino, D. Laux, "Evolution of the nuclear fuel mechanical properties with burn-up. An extensive european experimental program." Inter. Topical Meeting on Light Water Reactor Fuel Performance, Kyoto, Japan, oct 2-6, 2005.

[57]   C. B. Lee, B. G. Kim, J. S. Song, B. J.G., Y. H. Jung, "RAPID model to predict radial burnup distribution in LWR UO_2 fuel", J. Nucl. Mater., Vol. 282, 2-3, pp. 196-204, December 2000.

[58]   C. O'Carroll, C. T. Walker, J. van de Laar, C. Ott, R. Restani, "Validation of the TUBRNP model with the radial distribution of Plutonium in MOX fuel evaluated by SIMS and EMPA", Technical Committee Meeting on Water Reactor Fuel Element Modelling at High Burnup and Experimental Support, International Atomic Energy Agency, Bowness-on-Windermere, England, 19-23 September, 1994, pp. 313-325, IAEA-TECDOC-957.

[59]   Y. K. Bibilashvili, A. V. Medvedev, G. A. Khostov, S. M. Bogatyr, L. V. Korystine, "Development of the fission gas behaviour model in the START-3 code and its experimental support", Proc. Inter. Seminar on Fission Gas Behaviour in Water Reactor Fuels, Cadarache, France, September, 2000.

[60]   "Fuel Modelling at extended burnup (Fumex-II)", Report IAEA TECDOC, to be published in 2006.

[61]   K. Lassmann, A. Schubert, J. van de Laar, C. W. H. M. Vennix, "Recent developments of the TRANSURANUS code with emphasis on high burnup phenomena", IAEA Tech. Com. Meeting on Nuclear Fuel Behaviour Modelling at High Burnup, Vol. IAEA-TECDOC-1233, Lake Windermere, UK, 19-23 June, 2000, pp. 387-406.

[62]   M. Beauvy, "Uranium and Plutonium Oxides", Frederic Joliot - Otto Hahn Summer School on Nuclear Reactors "Physics, Fuels and Systems", Cadarache, France, August 23 - September 1, 2006.

[63]   A. Schubert, P. Van Uffelen, J. van de Laar, M. Sheindlin, L. Ott, "Present status of the MOX version of the TRANSURANUS code (F2.5)", Enlarged Halden Programme Group Meeting on High Burn-up

Fuel Performance, Safety and Reliability, Sandefjord, Norway, 9-14 May, 2004.

[64]   "Status and advances in MOX fuel technology", Technical report series no. 415, Report IAEA STI/DOC/010/415, 2003.

[65]   M. Billaux, J. van Vliet, "Impact of fuel heterogeneities on fission gas release for LWR U-Pu mixed oxide fuels", Res Mechanica, Vol. 17, pp. 41-57, 1986.

[66]   M. Ishida, Y. Korei, "Modeling and parametric studies of the effect of Pu-mixing heterogeneity on fission gas release from mixed oxide fuels of LWRs and FBRs", J. Nucl. Mater., Vol. 210, pp. 203-215, 1994.

[67]   Y. H. Koo, B. H. Lee, J. S. Cheon, D. S. Sohn, "Modeling and parametric studies of the effect of inhomogeneity on fission gas release in LWR MOX fuel", Annals of Nuclear Energy, Vol. 29, pp. 271-286, 2002.

[68]   P. Blanpain, M. Lippens, H. Schut, A. V. Federov, K. Bakker, "Helium solubility in UO_2 : the HARLEM project", Proc. Workshop Materials Models and Simulations for Nuclear Fuels, Nice, France, 1-2 June, 2006.

[69]   P. Blanpain, X. Thibault, J. Pages, "Recent results from the in reactor MOX fuel performance in France and improvement program", Inter. Topical Meeting on Light Water Reactor Fuel Performance, Portland, Oregon, USA, March 2-6, 1997, pp. 39-45.

[70]   T. Mitsugi, N. Kushida, K. Kikuchi, "Behaviour of MOX fuel irradiated in a thermal reactor", Inter. Topical Meeting on Light Water Reactor Fuel Performance, Portland, Oregon, USA, March 2-6, 1997, pp. 54-61.

[71]   M. Stan, "Materials models and simulations in support of nuclear fuels development", Report LA-UR-05-5652, Los Alamos National Laboratory, June 2005.

[72]   J. Crocombette, "Ab initio energetics of some fission products (Kr, I, Cs, Sr, He) in uranium dioxide", J. Nucl. Mater., Vol. 305, pp. 29-36, 2002.

[73]   J. Crocombette, F. Jollet, L. Nga, T. Petit, "Plane-wave pseudopotential study of point defects in uranium dioxide", Physical Review B, Vol. 64, pp. 104-107, 2001.

[74]   B. D. Wirth, G. R. Odette, J. Marian, L. Ventelon, J. A. Young-Vandersall, L. A. Zepeda-Ruiz, "Multiscale modeling of radiation damage in Fe-based alloys in the fusion environment", J. Nucl. Mater., Vol. 329-333, pp. 103-111, 2004.

[75]   L. Malerba, "Molecular dynamics study of displacement cascades in alpha-Fe: a critical review", J. Nucl. Mater., Vol. 351, 1-3, pp. 28-38, June 2006.

[76]   C. Domain, C. Becquart, L. Malerba, "Simulation of radiation damage in Fe alloys: an object kinetic Monte Carlo approach", J. Nucl. Mater., Vol. 335, pp. 121-145, 2004.

[77]   C. R. A. Catlow, "Fission gas diffusion in uranium dioxide", Proc. R. Soc. London, Vol. A 364, pp. 473-497, 1978.

[78]   S. Nicoll, H. Matzke, R. W. Grimes, "A comparatative study of the effect of Xe concentration on the behaviour of single Xe atoms in UO_2", J. Nucl. Mater., Vol. 226, pp. 51-57, 1995.

[79] G. Busker, R. W. Grimes, M. Bradford, "The diffusion of iodine and caesium in the UO_{2+x} lattice", J. Nucl. Mater., Vol. 279, pp. 46-50, 2000.

[80] C. Meis, A. Chartier, "Calculation of the threshold displacement energies in UO_2 using ionic potentials", J. Nucl. Mater., Vol. 341, 1, pp. 25-30, 2005.

[81] L. Van Brutzel, M. Raviromanantsoa, D. Ghaleb, "Displacement cascade initiated with the realistic energy of the recoil nucleus in UO_2 matrix by molecular dynamics simulation", J. Nucl. Mater., Vol. 354, 1-3, pp. 28-35, 2006.

[82] K. Kourosaki, K. Yamada, M. Uno, S. Yamanaka, K. Yamamoto, T. Namekawa, "Molecular dynamics study of mixed oxide fuels", J. Nucl. Mater., Vol. 294, pp. 160-167, 2001.

[83] E. Kroner, "Kontinuumstheorie der Versetzungen und Eigenspannungen", Springer-Verlag, 1958.

[84] J. Jonnet, B. Remy, P. Van Uffelen, "Stress function determination for dislocation configurations obtained from Kroner's theory", Theoretical and Applied Fracture Mechanics, Vol. 45, pp. 238-251, 4 May 2006.

Abstract

The present document contains the lecture notes of P. Van Uffelen for his presentation in the session "Fuel Development needs" of the 2006 Frédéric Joliot & Otto Hahn Summer School on Nuclear Reactors - Physics, Fuels and Systems – organised from 23rd August until 1st September 2006 in Cadarache (France).

In order to ensure the safe and economic operation of fuel rods, it is necessary to be able to predict their behaviour and life-time. The accurate description of the fuel rod's behaviour, however, involves various disciplines such as nuclear and solid state physics, metallurgy, ceramics, applied mechanics and the thermal heat transfer. The strong interrelationship of these disciplines calls for the development of computer codes describing the general fuel behaviour. Fuel designers and safety authorities rely heavily on this type of codes since they require minimal costs in comparison with the costs of an experiment or an unexpected fuel rod failure.

The first part of the lecture dedicated to fuel behaviour modelling reviews the basic equations implemented in the fuel rod performance codes, namely those for the heat generation and transfer from the center of the pellets to the coolant, the equations for the mechanical analysis of the fuel rod, and the equations for the behaviour of the gaseous fission products. In the second part of the lecture, advanced issues and future needs are discussed. Particular attention has been devoted to the probabilistic analysis in fuel performance calculations, to the role of the high burnup structure in UO_2 and MOX fuels, to the influence of the microstructure in mixed oxide fuels, and to the tendency to develop multi-time-scale approaches for both current and advanced nuclear fuels.